

Optimal determination of New Physics couplings: A comparative study

Subhaditya Bhattacharya,^a Sahabub Jahedi,^a Jose Wudka^b

^a*Department of Physics, Indian Institute of Technology Guwahati, Assam 781039, India*

^b*Department of Physics and Astrophysics, University of California, Riverside, California 92521, USA*

E-mail: subhab@iitg.ac.in, sahabub@iitg.ac.in, jose.wudka@ucr.edu

ABSTRACT: We study the determination of new physics (NP) parameters using the optimal observable technique (OOT) in situations where the standard model (SM) dominates over the NP effects, and when the NP dominates over the SM contribution, using the 2-Higgs doublet model as an illustrative example; for the case of SM domination we extend our results using an effective theory parameterization of NP effects. For the case of SM dominance we concentrate on $t\bar{t}$ production in an e^+e^- collider, while for the case of NP dominance we consider both $t\bar{t}$ production and pair production of charged scalars, also in an e^+e^- collider. We discuss the effects of the efficiency of background reduction, luminosity and beam polarization, and provide a comparison of the optimal uncertainties with those obtained using a standard χ^2 analysis of (Monte Carlo generated) collider data.

KEYWORDS: Specific BSM Phenomenology, Multi-Higgs Models, SMEFT, e^+e^- experiments

Contents

1	Introduction	1
2	Optimal uncertainties	3
3	Example of SM dominance: $t\bar{t}$ production at e^+e^- colliders	4
3.1	Collider analysis	9
3.2	1σ surfaces of EFT parameter uncertainties	11
3.3	Differentiation of hypotheses	12
3.4	Optimal versus standard χ^2	14
4	Example of NP dominance	16
4.1	$t\bar{t}$ production at e^+e^- colliders within flipped-2HDM	16
4.2	H^+H^- production at e^+e^- colliders	16
4.3	Collider analysis of the inert doublet model	19
4.4	1σ surfaces in the $a - b$ plane	20
4.5	Differentiation of models	21
4.6	Comparison between optimal and standard χ^2	22
5	Summary and Conclusions	25
A	OOT for large NP	26

1 Introduction

Although the Standard Model (SM) of particle physics is now complete after the discovery of Higgs Boson [1, 2] at the Large Hadron Collider (LHC), it leaves several questions unanswered, keeping the quest for new physics (NP) alive. However, LHC hasn't been able to pin down on any such NP yet, where searches are complicated by the huge hadronic activity and QCD backgrounds for many signals of NP. On the other hand, e^+e^- colliders are ideal for probing such cases. Accordingly, there are many proposals for such machines: the ILC [3–5], CLIC [6–8], CEPC [9, 10] and FCC [11, 12]. Precision measurements in particular, can be performed neatly at e^+e^- machines due to the complete knowledge of the centre-of-mass energy, availability of the beam polarization, and lack of hadronic activities and parton distribution function uncertainties. The top quark, being the heaviest SM particle, provides one of the most effective windows to probe NP; current measurements are still consistent with important deviations from SM prediction.

The Optimal Observable Technique (OOT) [13–16] is a powerful tool for determining the smallest statistical uncertainty to which any NP couplings can be determined in a given experimental environment; the degree to which any two models can be differentiated can also be predicted. The OOT has been applied to a variety of cases such as Higgs physics [17–19], top-quark physics at e^+e^- colliders [20–24], $\gamma\gamma$ colliders [25, 26], and $e\gamma$ colliders [27]. A few works have appeared using this approach in top-quark physics at the LHC [28–30] and various aspects of flavour physics [31–33]. Recently, the OOT has been used in studying heavy charged fermion [34] production and di-boson production [35, 36] at the e^+e^- collider. We also note that there exists some other statistical techniques, which uses optimisation for NP extraction, such as multivariate analysis [37–40], matrix method [41–44], etc.

Optimal uncertainties of NP couplings depend on the relative contributions of the NP and SM for the process under observation. In this paper we will consider two complementary situations: in the first the NP generates a subdominant correction to the SM, while in the second the NP dominates. These two cases can be realized, for example, in a 2-Higgs doublet model (see, *e.g.* [45, 46]), where, in the first, the scale of the non-SM scalars is large compared to the electroweak scale and with the collider energy; while in the second, that same scale is sufficiently low for non-SM particles to be directly produced. The specific illustrations we consider are, for the first case, $t\bar{t}$ production, and for the second, production of charged-scalar pairs.

The study of processes where the NP is not observed directly (*cf.* the first case above) is most conveniently done using the so-called SM effective field theory (SMEFT) approach. In our discussion below we will use this language when applicable, with the connection to a specific two-doublet model briefly spelled-out; the results thus obtained, even if motivated by a specific extension of the SM, will be more general. Within the SMEFT the Lagrangian takes the form

$$\mathcal{L}_{\text{eff}} = \mathcal{L}_{\text{SM}} + \frac{1}{\Lambda^{d-4}} \sum_i c_i O_i^d, \quad (1.1)$$

where c_i 's are the dimensionless “Wilson coefficients” and the O_i^d are gauge-invariant, dimension- d effective operators constructed using SM fields and their (covariant) derivatives; Λ denotes the scale of NP which, by consistency of this approach, must lie above the available energy. The lists of operators of dimension five [47], six [48, 49], seven [50, 51], eight [52–54] and nine [55–57] are already available. SMEFT approach has been used exhaustively to examine different properties of top-quark physics at the LHC [58–69], and also at the lepton colliders [21, 70–79].

The goals of the paper are, first, to provide an estimate of how well the coefficients can be measured for the two above cases; and second, to compare the optimal uncertainties with standard collider estimates in order to provide a measure of how far the experimental analysis can be improved (for this comparison we use Monte-Carlo generated ‘data’). The

collider analysis we use is basic, aimed at comparing and contrasting the results obtained by both methods; it can certainly be improved, a point on which we comment in section 5.

Our paper is organized as follows: in the next section we summarize the results of the OOT; we then study the case of $t\bar{t}$ production (section 3) as an example of SM dominance over the NP, and that of charged scalars where the NP dominates over the SM (section 4); a summary is presented in section 5.

2 Optimal uncertainties

In this section we provide a brief summary of the statistical uncertainties of the NP physics in the OOT approach. The results here are a straightforward extension of the OOT expression obtained in [15, 16, 34]; the derivation is summarized in the appendix.

The theoretical cross-section for a process involving both SM and NP contributions takes the general form

$$\mathcal{O}(\phi) = \frac{d\sigma_{\text{theo}}}{d\phi} = \frac{d\sigma_{\text{SM}}}{d\phi} + \sum_i g_i f_i(\phi), \quad (2.1)$$

where g_i are model-dependent coefficients (that, in general, are non-linear functions of the NP couplings), the f_i are functions of the phase-space variables ϕ ; for example, for a $2 \rightarrow 2$ scattering process such ϕ can be chosen as the scattering angle in the center-of-mass frame. The choice of the f_i 's are not unique although necessarily linearly independent, but all observable results are unambiguous.

We now consider a collider experiment with integrated luminosity $\mathfrak{L}_{\text{int}}$ and where the events of interest follow a Poisson distribution. In this case the optimal covariance matrix for the coefficients g_i is given by ,

$$V = \frac{1}{\mathfrak{L}_{\text{int}}} M^{-1}, \quad M_{ij} = \int \frac{f_i(\phi) f_j(\phi)}{\mathcal{O}(\phi)} d\phi. \quad (2.2)$$

If the SM contribution dominates the expression eq. (2.1), one can replace $\mathcal{O} \rightarrow \mathcal{O}_{\text{SM}} = d\sigma_{\text{SM}}/d\phi$ and the above expression reduces to the well-known result [15].

In a model where the coefficients take some specific values $g_i^{(0)}$, the corresponding statistical uncertainty for is determined by the χ^2 function given by

$$\chi^2 = \epsilon \sum_i \delta g_i \delta g_j (V_0^{-1})_{ij}, \quad \delta g_i = g_i - g_i^{(0)}, \quad V_0 = V|_{g=g^{(0)}}; \quad (2.3)$$

where ϵ is the efficiency for the process being considered; this factor takes into account the branching ratios of the produced particles to the signal states, as well as the effect of kinematic cuts used to segregate the signal from the SM background contamination. Specifically, the region $\chi^2 \leq n$ determines the region in parameter space around $g_i^{(0)}$ where the optimal statistical uncertainty of the g_i is below $\sqrt{n}\sigma$. For cases where the NP contribution is small,

i.e. $\mathcal{O} \simeq \mathcal{O}_{\text{SM}}$, V_0 will be independent of $g_1^{(0)}$, and so will the $\chi^2 \leq n$ region; however, in many cases of interest the SM dominates but the NP contribution to \mathcal{O} is not negligible, and the dependence of V_0 on $g_1^{(0)}$ may be important. It is worth mentioning that there are several studies applying the OOT to cases where NP effect is small, so that NP parameters can be neglected in the covariance matrix (V_0) [15, 19, 21–24, 27, 28].

3 Example of SM dominance: $t\bar{t}$ production at e^+e^- colliders

As an application of the OOT we consider $t\bar{t}$ production at an e^+e^- future collider like the ILC assuming any NP contributions are subdominant. These conditions are realized, for example, in the so-called “flipped” two-Higgs doublet model [80–85] (for a review see [86]) where one scalar doublet couples to down-type quarks, while the second doublet couples to leptons and up-type quarks. If this second doublet is assumed to be heavy ¹ it will generate an effective interaction of the form $(\bar{l}e)(\bar{q}u)$, where l, q are the lepton and quark left-handed doublets, and e, u the right-handed lepton and up-quark singlets, respectively. As noted in the Introduction, this situation can be studied in an effective theory approach, with the advantage that the results are not tied to a specific model. Thus, we consider first the possible low-energy manifestation of such UV complete model (*i.e.* below the scale of the heavy scalar) using an effective theory parameterization; within this context we will use the OOT to derive the minimum statistical uncertainty to which the Wilson couplings in the effective theory can be measured.

In the SM, pair-production of top-quark at the e^+e^- colliders is generated at tree-level by γ and Z mediation, as shown in the left side of fig. 1. The SMEFT contributions can be separated into two classes: those that modify the eeZ and ttZ vertices, and those that generate 4 fermion $eett$ vertices (right side of fig. 1).

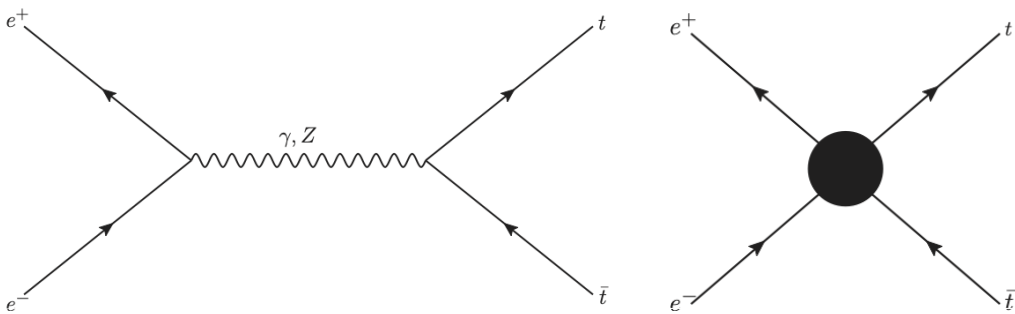


Figure 1: Top-quark pair production at e^+e^- collider. Left: SM contribution; Right: SMEFT contribution.

¹More specifically, we assume the second doublet has a small expectation value, large mass, and small mixing with the other doublet.

The relevant effective operators (in the so-called Warsaw-basis parameterization [49]) are:

group	Operator	vertex	
I	$Q_{\varphi l}^{(1)} = (i\varphi^\dagger D_\mu \varphi + \text{H.c.})(\bar{l}_p \gamma^\mu l_r)$	$\frac{1}{2}v^2 g_z \bar{e} \not{Z} P_L e$	(3.1)
	$Q_{\varphi l}^{(3)} = (i\varphi^\dagger \tau^I D_\mu \varphi + \text{H.c.})(\bar{l}_p \tau^I \gamma^\mu l_r)$	$-\frac{1}{2}v^2 g_z \bar{e} \not{Z} P_L e$	
	$Q_{\varphi e} = (i\varphi^\dagger D_\mu \varphi + \text{H.c.})(\bar{e}_p \gamma^\mu e_r)$	$\frac{1}{2}v^2 g_z \bar{e} \not{Z} P_R e$	
II	$Q_{\varphi q}^{(1)} = (i\varphi^\dagger D_\mu \varphi + \text{H.c.})(\bar{q}_p \gamma^\mu q_r)$	$\frac{1}{2}v^2 g_z \bar{t} \not{Z} P_L t$	
	$Q_{\varphi q}^{(3)} = (i\varphi^\dagger \tau^I D_\mu \varphi + \text{H.c.})(\bar{q}_p \tau^I \gamma^\mu q_r)$	$-\frac{1}{2}v^2 g_z \bar{t} \not{Z} P_L t$	
	$Q_{\varphi u} = (i\varphi^\dagger D_\mu \varphi + \text{H.c.})(\bar{u}_p \gamma^\mu u_r)$	$\frac{1}{2}v^2 g_z \bar{t} \not{Z} P_R t$	
III	$Q_{lq}^{(1)} = (\bar{l}_p \gamma_\mu l_r)(\bar{q}_s \gamma^\mu q_u)$	$(\bar{e} \gamma_\mu P_L e)(\bar{t} \gamma^\mu P_L t)$	
	$Q_{lq}^{(3)} = (\bar{l}_p \gamma_\mu \tau^I l_r)(\bar{q}_s \gamma^\mu \tau^I q_u)$	$-(\bar{e} \gamma_\mu P_L e)(\bar{t} \gamma^\mu P_L t)$	
	$Q_{lu} = (\bar{l}_p \gamma_\mu l_r)(\bar{u}_s \gamma^\mu u_u)$	$(\bar{e} \gamma_\mu P_L e)(\bar{t} \gamma^\mu P_R t)$	
	$Q_{qe} = (\bar{q}_p \gamma_\mu q_r)(\bar{e}_s \gamma^\mu e_u)$	$(\bar{e} \gamma_\mu P_R e)(\bar{t} \gamma^\mu P_L t)$	
	$Q_{eu} = (\bar{e}_p \gamma_\mu e_r)(\bar{u}_s \gamma^\mu u_u)$	$(\bar{e} \gamma_\mu P_R e)(\bar{t} \gamma^\mu P_R t)$	
IV	$Q_{lequ}^{(1)} = (\bar{l}_p^j e_r) \epsilon_{jk} (\bar{q}_s^k u_u)$	$-(\bar{e} P_R e)(\bar{t} P_R t)$	
	$Q_{lequ}^{(3)} = (\bar{l}_p^j \sigma_{\mu\nu} e_r) \epsilon_{jk} (\bar{q}_s^k \sigma^{\mu\nu} u_u)$	$-(\bar{e} \sigma_{\mu\nu} P_R e)(\bar{t} \sigma^{\mu\nu} P_R t)$	

where $g_z = \sqrt{g^2 + g'^2}$ and p, r, s, u are family indices.

In general, the operators in eq. (3.1) are generated by different types of NP so that they need not have a common scale Λ . The experimental constraints on the Zee coupling allow an $\sim 0.1\%$ deviation from the the SM prediction that corresponds to $\Lambda \sim 7$ TeV (for a unit Wilson coefficient) for group I operators [87]. The constraints on the ttZ coupling (group II) are significantly weaker $\Lambda \sim 1$ TeV [88]; the constraints on the 4-fermion operators (groups III and IV) will be of the same order.

Operators in group IV are unique in that, for the process at hand, they do not interfere with the SM, or with the operators in the other groups, and this will allow a future e^+e^- collider to differentiate their contributions from those generated by other types of new physics. These operators offer a convenient method to investigate a class NP effects by suppressing SM contributions in $t\bar{t}$ production for a judicious choice of beam polarization². It is one of the goals of this paper to illustrate this feature using the OOT as a tool; to simplify the discussion we will then consider the effects of these operators, ignoring those that may be generated by those in groups I, II and III. Our effective Lagrangian then takes the form

$$\mathcal{L}_{\text{eff}} = \frac{c_1}{\Lambda^2} Q_{lequ}^{(1)} + \frac{c_2}{\Lambda^2} Q_{lequ}^{(3)} + \text{H.c.}; \quad (3.2)$$

²As noted above, operators in group IV are generated by interesting types of new physics; for the current reaction their contributions do not interfere with the SM, which allows a clean evaluation of the effects of polarization – they produce $O(1/\Lambda^4)$ corrections. Operators in the I, II and III are generated by *different* types of new physics (*e.g.* additional Z gauge bosons) and do interfere with the SM, giving rise to $O(1/\Lambda^2)$ contributions. There are also contributions from dimension 8 operators which can generate $O(1/\Lambda^4)$ corrections as well, but these occur only in EFT-SM interference terms and do not correspond to the types of new physics being considered here.

where $c_{1,2}$ are dimensionless (Wilson) coefficients, and Λ is the scale of new physics³.

The helicity amplitude⁴ $M(\lambda_{e^-}, \lambda_{e^+}; \lambda_t, \lambda_{\bar{t}})$ for this process is given by

$$\begin{aligned}
M(\lambda, -\lambda; \lambda', -\lambda') &= e_0^2 \left(\frac{\lambda\lambda' + \cos\theta}{\beta_z^2} \right) \left[\frac{2}{3}\beta_z^2 - \left(\frac{4s_w^2 - 1 + \lambda}{4s_{2w}^2} \right) \left(1 - \frac{8}{3}s_w^2 - \beta_t\lambda' \right) \right], \\
M(\lambda, \lambda; \lambda', -\lambda') &= \frac{4c_2 m_t \sqrt{s}}{\Lambda^2} \lambda \sin\theta, \\
M(\lambda, -\lambda; \lambda', \lambda') &= \frac{2e_0^2 m_t \lambda' \sin\theta}{\sqrt{s}} \left[\frac{2}{3} - \left(\frac{4s_w^2 - 1 + \lambda}{4s_{2w}^2 \beta_z^2} \right) \left(1 - \frac{8}{3}s_w^2 \right) \right], \\
M(\lambda, \lambda; \lambda', \lambda') &= \frac{s}{2\Lambda^2} (\lambda\lambda'\beta_t - 1) (c_1 + 4c_2\lambda\lambda' \cos\theta); \tag{3.3}
\end{aligned}$$

where $\lambda_i = \pm 1$ indicates the helicity of particle i , e_0 the $U(1)_{\text{em}}$ coupling constant, \sqrt{s} the CM energy, $s_w = \sin(\theta_w)$, $s_{2w} = \sin(2\theta_w)$ (θ_w denotes the weak mixing angle), m_t the top-quark mass, m_z the Z -boson mass and

$$\beta_z = \sqrt{1 - \frac{m_z^2}{s}}; \quad \beta_t = \sqrt{1 - \frac{4m_t^2}{s}}. \tag{3.4}$$

In the above expressions, electron mass has taken to be zero; we also assumed that $c_{1,2}$ are real, if this is not the case then one must replace $c_a \rightarrow \mathbf{Re}c_a + i\lambda_e \mathbf{Im}c_a$. We note here that, for zero electron mass, the SM contributes only to the opposite helicity amplitudes $\lambda_{e^-} = -\lambda_{e^+}$, whereas scalar and tensor mediated effective operators contribute only to same helicity amplitudes, so there is no EFT-SM interference; this is not the case for possible contributions from operators in groups I-III in eq. (3.1).

The corresponding differential cross-section when the e^\pm beams have partial polarizations P_{e^\pm} (with $-1 \leq P_{e^\pm} \leq 1$) is given by

$$\frac{d\sigma(P_{e^+}, P_{e^-})}{d\Omega} = \sum_{\lambda_e^+ = \pm 1} \sum_{\lambda_e^- = \pm 1} \frac{(1 + \lambda_{e^-} P_{e^-})(1 + \lambda_{e^+} P_{e^+})}{4} \left(\frac{d\sigma}{d\Omega} \right)_{\lambda_{e^-}, \lambda_{e^+}}; \tag{3.5}$$

where $(d\sigma/d\Omega)_{\lambda_{e^-}, \lambda_{e^+}}$ is the cross section obtained from eq. (3.3) by summing over $\lambda_t, \lambda_{\bar{t}}$. For $s \gg m_t^2$ and $s_w^2 \simeq 0.25$ it is easy to see that the SM contribution to the total cross section has the form

$$\sigma(P_{e^+}, P_{e^-})_{\text{SM}} \propto 1 - \mathbf{a}^2 + (\mathbf{a} - P_{e^-})(\mathbf{a} + P_{e^+}), \quad \mathbf{a} \sim 0.0652; \tag{3.6}$$

which vanishes when $P_{e^+} = P_{e^-} = \pm 1$ and has a maximum when $P_{e^\pm} = \pm 1$; the SM polarized cross section lies above the unpolarized one when $P_{e^-} \lesssim \mathbf{a}$ and $P_{e^+} \gtrsim -\mathbf{a}$, or $P_{e^-} \gtrsim \mathbf{a}$ and $P_{e^+} \lesssim -\mathbf{a}$.

³Within the context of the flipped two-Higgs doublet model, Λ denotes the scale of the heavy scalar and c_1 the product of its Yukawa couplings to the leptons and up-type quarks.

⁴For the helicity amplitude calculation see [89].

Explicitly, the SM contribution is given by

$$\begin{aligned}
\frac{d\sigma_{\text{SM}}}{d\Omega} = & \frac{\alpha_0^2(1 - P_{e^-}P_{e^+})}{3s} \left\{ 1 + \mathbf{C}(\xi_1 - P_{\text{eff}}\xi_2) + \frac{1}{4}(\xi_1^2 - 2P_{\text{eff}}\xi_1\xi_2 + \xi_2^2) \left(\mathbf{C}^2 + \frac{\beta_t^2}{2 - \beta_t^2} \right) \right. \\
& - \left[\xi_2(1 + \mathbf{C}\xi_1) - \frac{1}{4}P_{\text{eff}} \left(4\xi_1 - (2\xi_1^2 - \xi_2^2)\mathbf{C} \right) \right] \beta_t \cos \theta + \\
& \left. + \left[1 + \mathbf{C}(\xi_1 - P_{\text{eff}}\xi_2) + \frac{2\mathbf{C} + 1}{4}(\xi_1^2 - 2P_{\text{eff}}\xi_1\xi_2 + \xi_2^2) + \frac{\mathbf{C}(2 - \mathbf{C})}{2}P_{\text{eff}}\xi_1\xi_2 \right] \beta_t^2 \cos^2 \theta \right\}; \tag{3.7}
\end{aligned}$$

where

$$P_{\text{eff}} = \frac{P_{e^-} - P_{e^+}}{1 - P_{e^-}P_{e^+}}, \quad \xi_1 = \frac{1}{2s_{2\mathbf{w}}^2\beta_z^2}, \quad \xi_2 = \frac{4s_{\mathbf{w}}^2 - 1}{2s_{2\mathbf{w}}^2\beta_z^2}, \quad \mathbf{C} = 3 - 12s_{\mathbf{w}}^2; \tag{3.8}$$

and, using the notation of eq. (2.1), effective operator contribution is determined by the following choice of f_i and g_i :

$$\begin{aligned}
\{f_1, f_2, f_3\} = & \frac{3\beta_t s}{256\pi^2\Lambda^4} \left\{ (1 + \beta_t^2), 16\beta_t \cos \theta, 32\beta_t^2 \cos^2 \theta \right\}, \\
\{g_1, g_2, g_3\} = & (1 + P_{e^-}P_{e^+}) \left\{ \left(c_1^2 + 16\frac{1 - \beta_t^2}{1 + \beta_t^2}c_2^2 \right), -c_1c_2, c_2^2 \right\}. \tag{3.9}
\end{aligned}$$

We plot in fig. 2 this differential cross section and the associated cross section for various choices of the model parameters and beam polarizations. As expected, the SM cross section decreases as the CM energy \sqrt{s} increases, and the polarized SM cross section for $P_{e^\pm} = \begin{smallmatrix} -5\% \\ +80\% \end{smallmatrix}$ is smaller than the unpolarized one, in accordance with eq. (3.6). We therefore will use this choice of beam polarizations for the optimal estimation of the Wilson coefficients, and compare it to that with unpolarized beams.

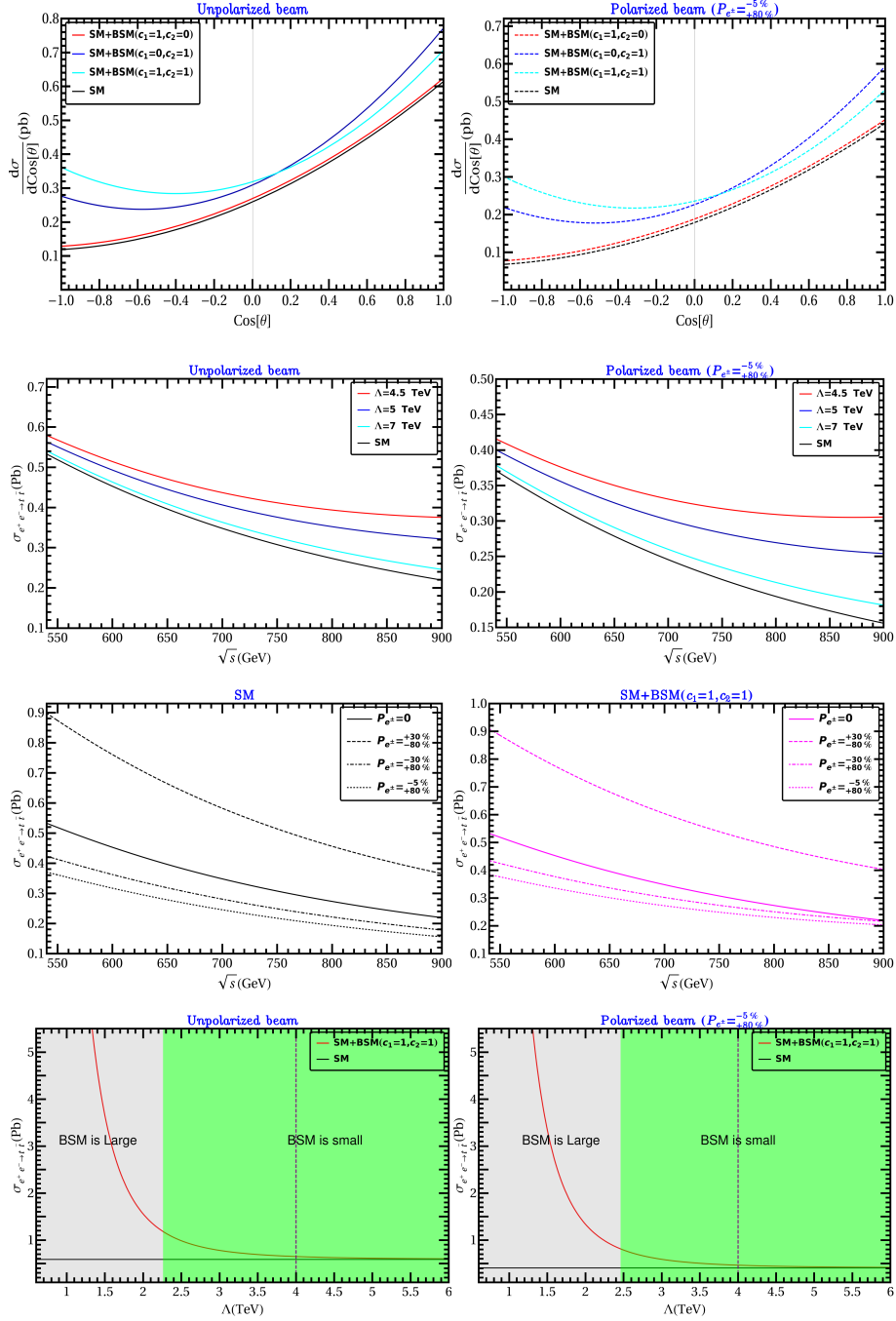


Figure 2: Plots of the $e^+e^- \rightarrow t\bar{t}$ cross-section. Top row: angular dependence for CM energy $\sqrt{s} = 500$ GeV, and different values of Λ for unpolarized (left) and polarized with $P_{e^\pm} = \begin{smallmatrix} -5\% \\ +80\% \end{smallmatrix}$ (right) beams. Second row: total cross section as a function of \sqrt{s} for $c_1 = c_2 = 1$ and several values of Λ , for unpolarized (left) and unpolarized (right) beams. Third row: dependence on the beam polarization for the SM (left) and the SM + EFT with $c_1 = c_2 = 1$ and $\Lambda = 4$ TeV (right). Bottom row: comparison of the SM total cross section (black horizontal line) with the SM + EFT with $c_1 = c_2 = 1$ as a function of Λ for unpolarized (left) and polarized (right) beams; the region labeled “BSM small” corresponds to $\sigma_{\text{SM+EFT}} > 2\sigma_{\text{SM}}$.

It also evident that as Λ increases the total cross-section approaches the SM value. We identify a value $\Lambda = \Lambda_{\text{boundary}}$ corresponding to $\sigma_{\text{tot}} = 2\sigma_{\text{SM}}$, so that the process is SM-dominated when $\Lambda > \Lambda_{\text{boundary}}$; using fig. 2 we find $\Lambda_{\text{boundary}} \sim 2 \text{ TeV}$ and, being interested in situations where the EFT represents a correction to the SM, we will consider NP scales above this value. This also shows why $t\bar{t}$ production is such an effective process to probe NP above TeV scale. For our explicit calculations we use the following collider parameters:

$$\Lambda = 4 \text{ TeV}; \quad \sqrt{s} = 500 \text{ GeV}; \quad \mathfrak{L}_{\text{int}} = 1000 \text{ fb}^{-1}.$$

3.1 Collider analysis

In this section, we provide an event level signal and background analysis of top quark pair production at e^-e^+ machine. Our main goal here is to determine the efficiency ϵ with which we approximate the optimal observable.

As noted earlier, the SM process is mediated by Z or photon in s-channel exchange, while the NP effects we consider are generated by a contact 4-fermion interaction; as in the previous sections we will restrict ourselves to the NP effects in eq. (3.2). We will consider only the leptonic decays of the W bosons that follow from the decay of the $\bar{t}t$ pair, namely,

$$e^+e^- \longrightarrow t\bar{t} \rightarrow (bW^+) (\bar{b}W^-) \rightarrow (bl^+\nu_l) (\bar{b}l^-\bar{\nu}_l); \quad l, l' = e, \mu, \quad (3.10)$$

(see fig. 3). Thus the signature will be two opposite-sign leptons of same/different flavors + two b jets+ missing energy (\cancel{E}). The leading (non-interfering) SM background contributions are generated by Zh , ZZ and W^+W^-Z production.

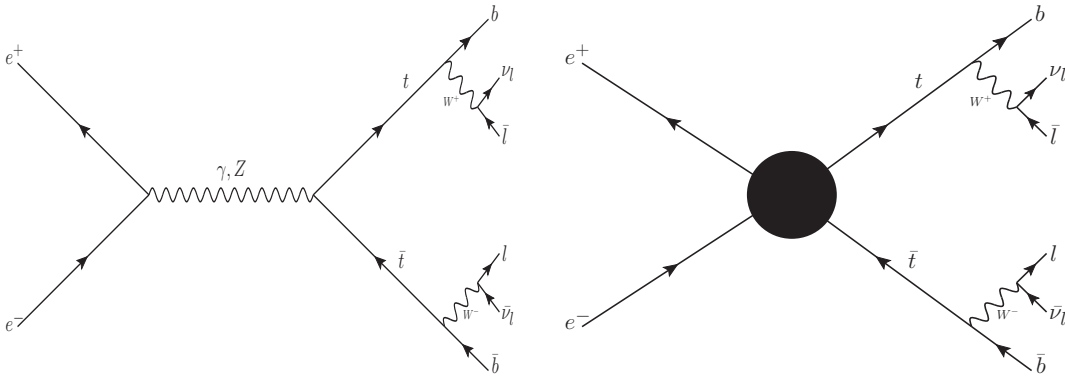


Figure 3: Production and decay of top-quark at e^+e^- colliders for $2l + 2b + \text{missing energy}$ signal.

We follow a standard approach, generating parton-level signal events using CalcHEP [90]; the events are then showered and analyzed using Pythia [91]. For event reconstruction, and lepton and jet identification we use the following criteria:

BPs	Input model	Cross-section (fb)	
		$P_{e^\pm} = 0$	$P_{e^\pm} = \begin{smallmatrix} -5\% \\ +80\% \end{smallmatrix}$
BP1	$c_1 = 1, c_2 = 0$	597.8	415.4
BP2	$c_1 = 0, c_2 = 1$	645.7	461.4
BP3	$c_1 = 1, c_2 = 1$	651.9	467.4

Table 1: Total cross-section at e^+e^- collider for different benchmark points for unpolarized and polarized $P_{e^\pm} = \begin{smallmatrix} -5\% \\ +80\% \end{smallmatrix}$ beams with $\sqrt{s} = 500$ GeV. All the benchmark points have $\Lambda = 4$ TeV.

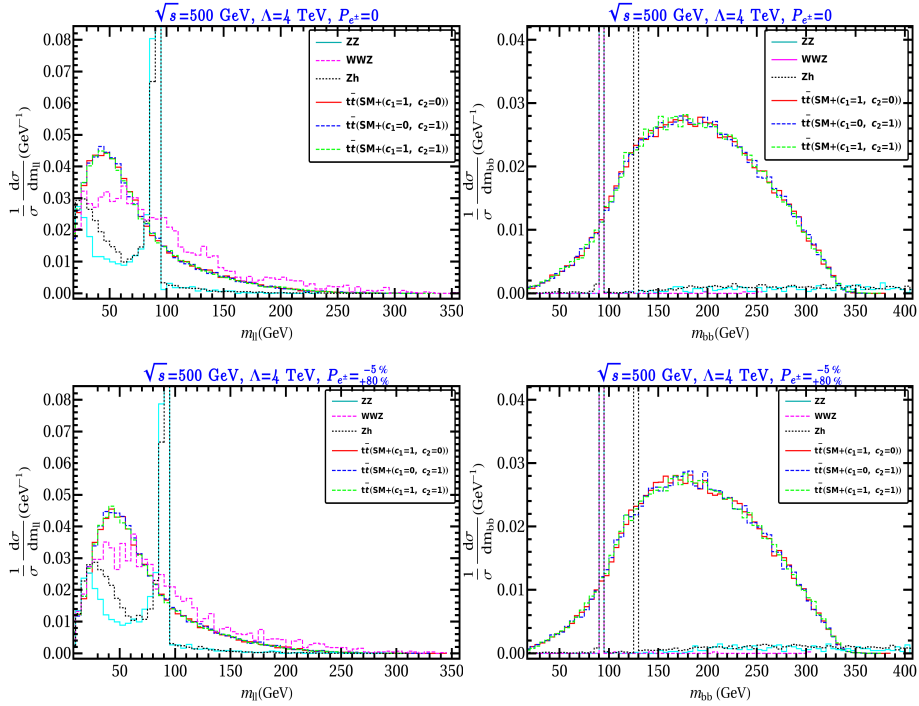


Figure 4: Invariant di lepton mass (m_{ll}) (left), Invariant di b-jet mass (m_{bb}) distributions (right) for $2l + 2b +$ missing energy final state coming from $t\bar{t}$ signal with EFT ($\Lambda = 4$ TeV) as well as dominant SM backgrounds at the e^+e^- collider with $\sqrt{s} = 500$ GeV. Top panel: Unpolarized beams; bottom panel: polarized beams $P_{e^\pm} = \begin{smallmatrix} -5\% \\ +80\% \end{smallmatrix}$.

- Events must have two opposite-sign leptons, and two b jets; the b -tagging efficiency is chosen to be 0.6 in accordance with the ILC TDR [3].
- Lepton transverse momentum: $p_T^l > 10$ GeV.
- Light jet transverse momentum: $p_T^j > 20$ GeV.

- Leptons and light jets must be isolated: $\Delta R_{ll'} > 0.2$, $\Delta R_{jl} > 0.4$ and $\Delta R_{jj'} > 0.4$.
- Exclude events where the dilepton invariant mass is in the range $75 \text{ GeV} < m_{ll} < 105 \text{ GeV}$ to reduce the $Z \rightarrow \ell^+ \ell^-$ background.
- Exclude events where the $b-\bar{b}$ invariant mass is in the range $115 \text{ GeV} < m_{bb} < 135 \text{ GeV}$, to reduce $h \rightarrow b\bar{b}$ contamination.

where we defined $\Delta R = \sqrt{\Delta\eta^2 + \Delta\phi^2}$ as the usual distance in the rapidity (η) - azimuthal angle (ϕ) plane. The invariant mass cuts are designed to exclude the SM background; the values selected are based on the event distributions plotted in fig. 4.

Using these selection criteria we find the efficiency ϵ as the ratio of observed cross section σ^{FS} to the production cross section σ^{prod} :

$$\epsilon = \frac{\sigma^{\text{FS}}}{\sigma^{\text{prod}}}. \quad (3.11)$$

For the benchmark points in table 1 we find $\epsilon \sim 0.008$, roughly independent of polarization. In the following we take a conservative approach and use $\epsilon = 0.001$ or $\epsilon = 0.005$.

3.2 1σ surfaces of EFT parameter uncertainties

Using eq. (2.3), we define the optimal 1σ region of the statistical uncertainties of the EFT parameters $c_{1,2}$ for the above described reaction. We choose three different combinations of the NP coupling seed values: *i*) $c_1^0 = 1, c_2^0 = 0$, *ii*) $c_1^0 = 0, c_2^0 = 1$, and *iii*) $c_1^0 = 1, c_2^0 = 1$. The 1σ regions are plotted in fig. 5 for various choices of input values $c_i^{(0)}$ and beam polarizations in $\Delta c_i - \Delta c_j$ plane where $\Delta c_i = c_i - c_i^0$. For this calculation we choose $\sqrt{s} = 500 \text{ GeV}$ and $\mathcal{L}_{int} = 1000 \text{ fb}^{-1}$. Note that, even though the SM dominates, the NP effects are significant even for $\Lambda = 4 \text{ TeV}$.

The 1σ uncertainties for different combination of input values are listed in table 2, while 1σ surfaces are shown in fig. 5. The polarization of the initial beams in the lepton collider play a crucial role in determining the uncertainties of NP couplings. Precise extraction of NP relies on reducing the SM contribution and/or enhancing BSM contribution to the specific process. The uncertainties of NP couplings for different choices of beam polarization (within the possible ranges in accordance to collider TDR) are shown in the bottom right of fig. 5. For $(P_{e\pm} = \begin{smallmatrix} +5\% \\ -80\% \end{smallmatrix})$, both SM and BSM contribution to the top-quark pair production increase, while if we flip the polarization sign, both contributions will decrease. But we observe that $(P_{e\pm} = \begin{smallmatrix} -5\% \\ +80\% \end{smallmatrix})$ provides more precise $\Delta c_i - \Delta c_j$, which implies that the reduction of SM contribution is larger than the reduction in BSM contribution. We note that for $(P_{e\pm} = \begin{smallmatrix} +5\% \\ -80\% \end{smallmatrix})$ choice of polarization combination, NP uncertainties are $\sim 10 - 20\%$ smaller compared to unpolarized beam. We also note that in all cases the uncertainties for the tensor operator coefficient c_2 are smaller than for the scalar one, as the tensor operator provides larger BSM contribution to $t\bar{t}$ production than the scalar operator. As Λ increases, BSM contribution to

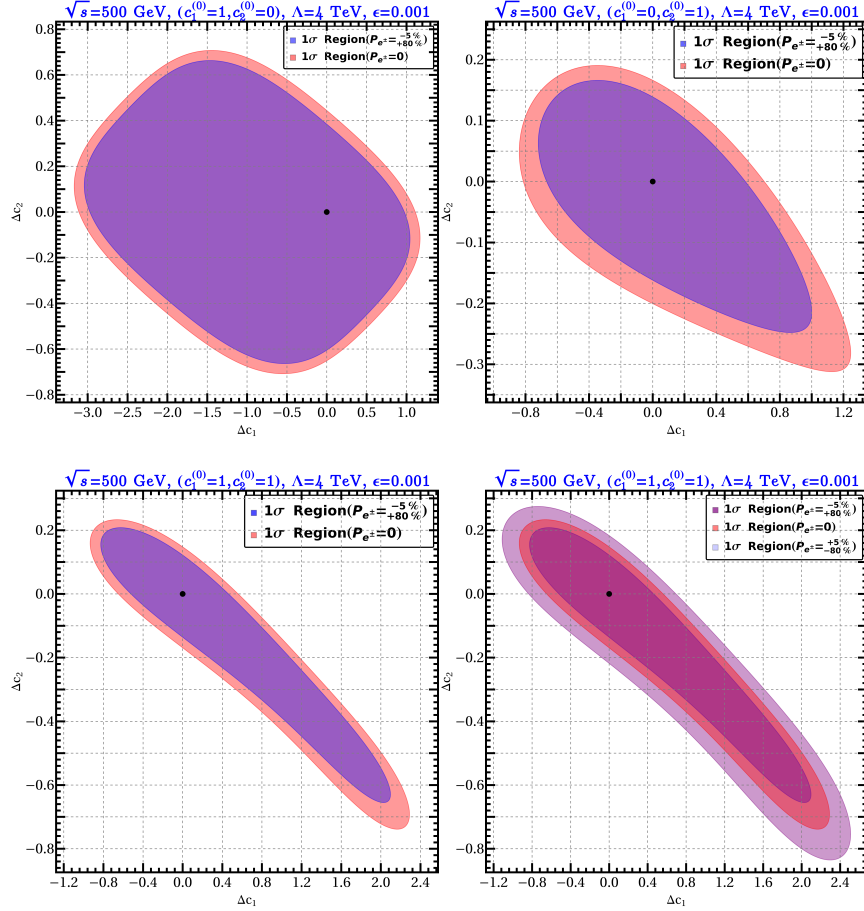


Figure 5: Optimal $1\text{-}\sigma$ regions in $\Delta c_1 - \Delta c_2$ plane for various choices of EFT parameters and choices of beam polarization. See figure inset and heading for details.

the production cross-section is reduced, as a result, the uncertainties of the NP couplings are also increased. This behaviour is illustrated in fig. 6.

The OOT done here is primarily signal-based, where we assume that the non-interfering background effects are negligible, which is true to a great extent. However, uncertainty of NP couplings will increase when we include these remaining background effects. We take into account these effects by choosing a lower efficiency ($\epsilon = 0.001$) than the one derived when ignoring such backgrounds ($\epsilon = 0.008$).

3.3 Differentiation of hypotheses

Seed parameters	$P_{e^\pm} = 0$				$P_{e^\pm} = \begin{smallmatrix} -5\% \\ +80\% \end{smallmatrix}$			
	$\epsilon = 0.005$		$\epsilon = 0.001$		$\epsilon = 0.005$		$\epsilon = 0.001$	
	$\pm\Delta c_1$	$\pm\Delta c_2$	$\pm\Delta c_1$	$\pm\Delta c_2$	$\pm\Delta c_1$	$\pm\Delta c_2$	$\pm\Delta c_1$	$\pm\Delta c_2$
$c_1^{(0)} = 1, c_2^{(0)} = 0$	+0.52	+0.32	+1.16	+0.71	+0.46	+0.29	+1.03	+0.66
	-1.41	-0.32	-3.18	-0.71	-1.37	-0.15	-3.06	-0.66
$c_1^{(0)} = 0, c_2^{(0)} = 1$	+0.55	+0.08	+1.24	+0.19	+0.44	+0.07	+1.00	+0.16
	-0.37	-0.14	-0.84	-0.31	-0.32	-0.11	-0.72	-0.25
$c_1^{(0)} = 1, c_2^{(0)} = 1$	+1.02	+0.10	+2.29	+0.23	+0.55	+0.09	+1.24	+0.19
	-0.42	-0.33	-0.94	-0.74	-0.37	-0.14	-0.84	-0.31

Table 2: Optimal 1σ statistical uncertainties of the c_1, c_2 couplings for unpolarized and polarized $P_{e^\pm} = \begin{smallmatrix} -5\% \\ +80\% \end{smallmatrix}$ beams, and two values of ϵ ; we used the parameters in eq. (3.10).

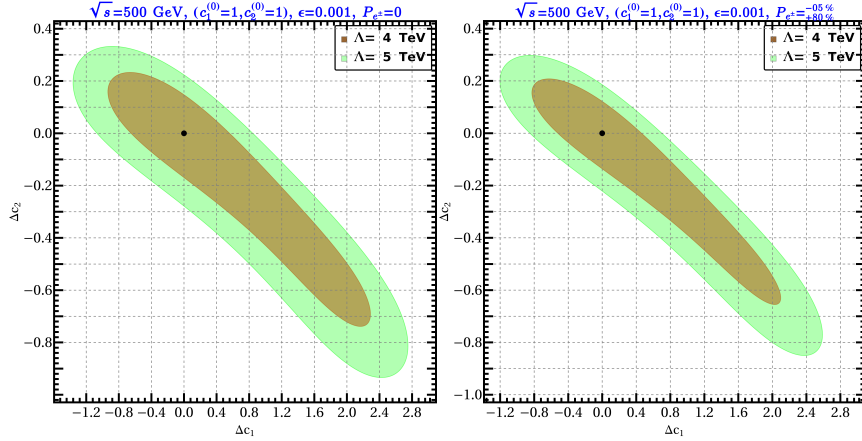


Figure 6: 1σ surfaces in $\Delta c_1 - \Delta c_2$ plane for two choices of Λ and unpolarized (left) and polarized $P_{e^\pm} = \begin{smallmatrix} -5\% \\ +80\% \end{smallmatrix}$ (right) beams. See figure inset and heading for details.

An important feature of the OOT is that it provides a quantitative estimate of the degree to which a ‘base hypothesis’ (characterized by NP coefficients $g_i^{(0)}$) can be distinguished from an alternate one (characterized by \bar{g}_i). To this end we define the statistical significance by

$$\Delta\sigma^2(g^{(0)}; \bar{g}) = \epsilon \sum_{i,j} (g_i^0 - \bar{g}_i) (g_j^0 - \bar{g}_j) (V_0^{-1})_{ij}, \quad V_0 = V(g = g^0); \quad (3.12)$$

with V_0 defined in eq. (2.3), and $g_i^0 = g_i(c_1^0, c_2^0)$ and $\bar{g}_i = g_i(\bar{c}_1, \bar{c}_2)$ as in eq. (3.9).

As an example, we consider $c_1^{(0)} = c_2^{(0)} = 0$ as the base hypothesis (that corresponds to the SM), and various other choices of the seed values of NP couplings (given in the previous

model	ϵ	\mathcal{L}_{int} (fb $^{-1}$)	significance($\Delta\sigma$)	
			$P_{e^\pm = 0}$	$P_{e^\pm = \begin{smallmatrix} -5\% \\ +80\% \end{smallmatrix}}$
$\bar{c}_1 = 1$ $\bar{c}_2 = 0$	0.001	1000	0.29	0.35
	0.001	2000	0.41	0.49
	0.005	1000	0.69	0.78
$\bar{c}_1 = 0$ $\bar{c}_2 = 1$	0.001	1000	2.77	3.36
	0.001	2000	3.92	4.75
	0.005	1000	6.19	7.51
$\bar{c}_1 = 1$ $\bar{c}_2 = 1$	0.001	1000	3.93	4.83
	0.001	2000	5.56	6.82
	0.005	1000	8.79	10.80

Table 3: Statistical significance $\Delta\sigma$ (see eq. (3.12)) of several hypotheses \bar{c}_1, \bar{c}_2 with respect to the SM.

section) as alternative hypotheses. The degree of statistical differentiation of the alternate hypotheses from the base hypothesis are shown in fig. 7 and listed in table 3, for both unpolarized and polarized beams. For unpolarized beams, hypothesis I ($\bar{c}_1 = 1, \bar{c}_2 = 0$) is indistinguishable from the SM even if we choose $\epsilon = 0.005$ and $\mathcal{L}_{\text{int}} = 2000 \text{ fb}^{-1}$. With $\epsilon = 0.001(0.005)$ and $\mathcal{L}_{\text{int}} = 2000 \text{ fb}^{-1}$, hypothesis II ($\bar{c}_1 = 0, \bar{c}_2 = 1$) lies beyond 3σ (5σ) the exclusion (discovery) limit. Due to larger BSM contribution, hypothesis III ($\bar{c}_1 = 1, \bar{c}_2 = 1$) is easier to distinguish than the other two hypotheses. Appropriate beam polarization, larger ϵ and high luminosity help the differentiation become more significant.

3.4 Optimal versus standard χ^2

In this section we provide a comparison of the optimal coefficient uncertainties with those obtained using a basic analysis of collider data. To this end we imagine a collider experiment where the data obtained is organized in a number of bins $j = 1, 2, \dots, J$. We consider the differential cross-section with respect to the opening angle of the outgoing particles in the CM frame as our observable for this binned analysis (as was done in the OOT approach). We denote by N_j^{obs} the number of events in the j -th bin, and $N_j^{\text{theo}}(g_i)$ the theoretical prediction for this number; using this we define [92]

$$\chi^2 = \sum_j^{\text{bins}} \left(\frac{N_j^{\text{obs}} - N_j^{\text{theo}}(g_i)}{\sqrt{N_j^{\text{obs}}}} \right)^2. \quad (3.13)$$

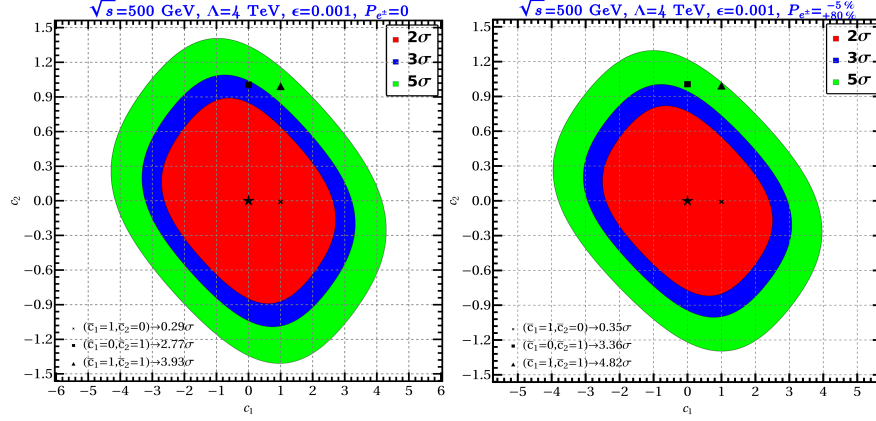


Figure 7: Statistical significance (*cf.* eq. (3.12)) $\Delta\sigma \leq 2, 3, 5$ (respectively, red, blue and green areas) of alternate models with respect to the SM for unpolarized (left) and polarized $P_{e\pm} = \begin{smallmatrix} -5\% \\ +80\% \end{smallmatrix}$ beams (right); also noted the statistical significance of 3 specific models. See figure inset and heading for details of the parameter choices.

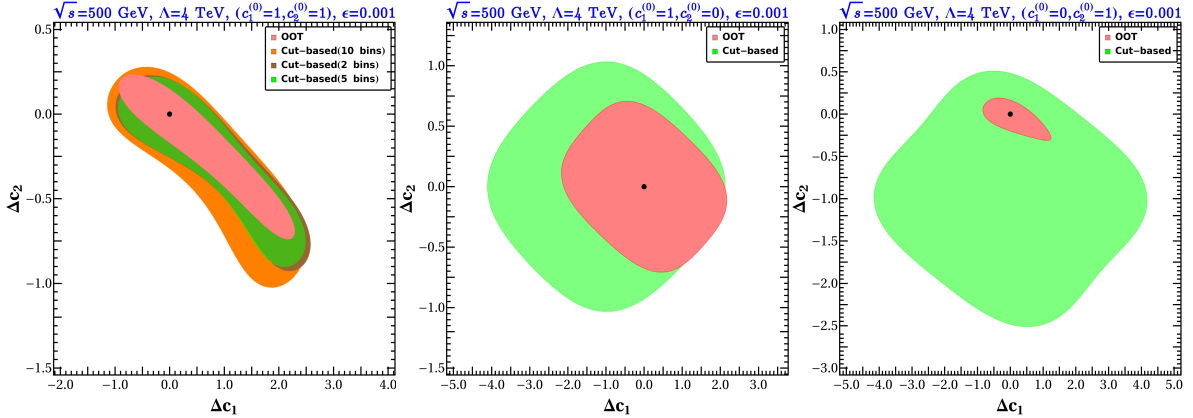


Figure 8: Comparison of 1σ surfaces in $\Delta c_1 - \Delta c_2$ plane between OOT (light red) and cut-based analysis as in eq. (3.13) (in green) for unpolarized beams.

From this we define the 1σ regions in parameter space by the condition $\chi^2 \leq 1$. In our case the N_j^{obs} are obtained using a numerical simulation that implements all the cuts described in section 3.1. The results for three choices of model parameters, and the comparison with the corresponding OOT results are presented in fig. 8. The χ^2 statistic defined in eq. (3.13) depends on the number of bins, a dependence that is also examined in fig. 8; we find that choosing 5 bins provides the most constrained parameter space⁵ and thus we use this choice in the following examples. These results give a measure of the degree to which the analysis

⁵This choice provides a balance between the number of events with the statistical fluctuations in each bin.

based on eq. (3.13) can be improved. In this case, as BSM contribution is less than SM to the signal final state, the statistical fluctuation in each bin is large, as a consequence, uncertainties in NP couplings estimated from binned analysis is worse than the OOT uncertainties.

4 Example of NP dominance

We now consider the determination of NP parameters in cases where the NP dominates over the SM; specifically, we will consider the production of new particles at an e^+e^- collider. For this a specific model must be selected, and we will use the well-understood extension of the SM where an additional doublet is added to the scalar sector, the two-Higgs doublet model⁶ (2HDM). As noted in section 3, the so-called ‘flipped’ 2HDM [80–86] can be used to describe the type of NP effects considered in that section.

The new particles in the 2HDM are a neutral CP-even scalar, a neutral CP-odd scalar, and a pair of charged scalars H^\pm ; we will also assume the presence of right-handed neutrinos N_R and assume that the N_R and H^\pm are light enough to be produced at the e^+e^- collider. We then will study the degree to which this collider can be expected to determine some of the couplings associated with this extension of the SM.

4.1 $t\bar{t}$ production at e^+e^- colliders within flipped-2HDM

We first briefly revisit the process considered in section 3, assuming now that the NP can be directly produced in colliders. In this case the contact interaction on the right-hand diagram on fig. 1 is replaced by the heavy scalar exchange diagram in fig. 9. We consider flipped 2HDM to elucidate this scenario. This model does not generate the effective interaction $Q_{lequ}^{(3)}$ in eq. (3.2), so that $c_2 = 0$. The Yukawa couplings to the CP-even heavy Higgs (H) are given by [86],

$$-\mathcal{L}_{\text{yuk}} = \frac{m_f}{v} y_f \bar{f} f H, \quad (4.1)$$

where $y_f = \cos(\beta - \alpha) - \sin(\beta - \alpha)\kappa_f$, with $\kappa_f = \cot\beta = v_1/v_2$ and α is the angle associated with the diagonalization of the neutral CP-even scalar mass matrix.

For this model $c_1 = \frac{m_e m_t}{v^2} k_f$. In order to estimate the uncertainty of this NP coupling we will consider the resonant production of H and its subsequent decay $\rightarrow t\bar{t}$. In the numerical analysis, we consider heavy Higgs mass $m_H = 500$ GeV, $\sin(\beta - \alpha) \sim 1$ in the decoupling limit and small $\tan\beta$ (~ 0.5). In this case we find $c_1 = 5.7 \times 10^{-7}$. Comparing uncertainty in c_1 , Δc_1 in the flipped-2HDM is smaller than in the EFT scenario due to a greater NP contribution to $t\bar{t}$ production.

4.2 H^+H^- production at e^+e^- colliders

We consider next the pair production of H^\pm which provides an additional channel to probe the NP in this model in which the NP contribution dominates. We assume that the H^\pm have

⁶For a recent review see [86, 93, 94].

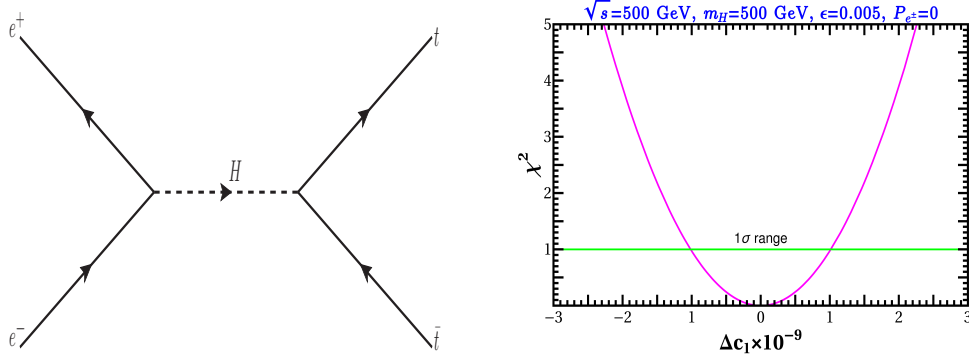


Figure 9: Left: NP contribution to $e^+e^- \rightarrow t\bar{t}$ in a flipped 2HDM; where H denotes a heavy scalar. Right: dependence of χ^2 (eq. (2.3)) on the NP coefficient uncertainty Δc_1 , when $c_1^{(0)} = 5.71 \times 10^{-7}$, with the 1σ bound indicated.

the standard minimal coupling to the photon,

$$H^+(p_4)H^-(p_3)\gamma : -ie_0(p_4^\mu - p_3^\mu), \quad (4.2)$$

and parameterize the leptonic-Yukawa⁷ and Z couplings as follows:

$$\begin{aligned} H^+(p_4)H^-(p_3)Z &: -ia(p_4^\mu - p_3^\mu), \\ e^+N_RH^- &: b; \end{aligned} \quad (4.3)$$

where, p_3 and p_4 are the incoming momenta of H^- and H^+ , respectively. For definiteness we will consider three different models : the flipped 2 HDM or inert doublet model (IDM) (doublet) [95], the type-II seesaw model (triplet) [96], and the scotogenic model [97]; these are characterized by⁸,

Model	a	b	
Flipped 2 HDM/Inert-doublet (IDM):	$e_0 \cot(2\theta_w) = 0.21$	0	(4.4)
Scotogenic:	$e_0 \cot(2\theta_w) = 0.21$	0.1	
Type II seesaw:	$e_0 \tan(\theta_w) = 0.17$	0	

As a concrete application we will consider H^+H^- pair-production at a linear e^+e^- collider; the relevant diagrams are shown in fig. 10. The corresponding helicity amplitudes, $M'(\lambda_{e^-}, \lambda_{e^+})$, are easily obtained: $M'(\lambda, \lambda) = 0$, and

$$M'(\lambda, -\lambda) = i \left[e_0^2 + ae_0 \left(\frac{4s_w^2 - 1}{2s_{2w}} - \lambda \frac{1}{2s_{2w}} \right) \frac{s}{s - m_Z^2} + \frac{(1 + \lambda)b^2}{4} \frac{s}{t - m_N^2} \right] \beta_{H^+} \sin \theta; \quad (4.5)$$

⁷We assume that the masses of any other heavy neutrinos are large enough to have negligible effects at the colliders being considered.

⁸Here, b is a free parameter.

where θ is the scattering angle of H^\pm from the axis of collision, $\beta_{H^\pm} = \sqrt{1 - 4m_{H^\pm}^2/s}$, and

$$t = \frac{s}{2} (1 + \beta_{H^\pm} \cos \theta) + m_{H^\pm}^2. \quad (4.6)$$

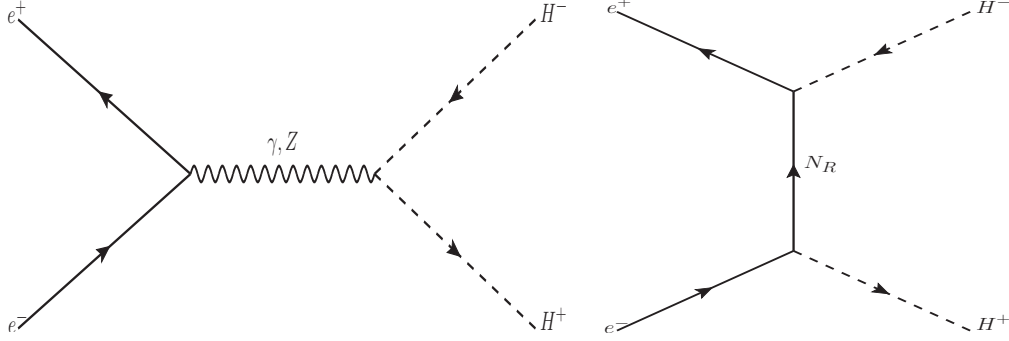


Figure 10: Leading pair-production mechanism for singly charged scalar pairs (H^\pm) at an e^\pm collider.

In the numerical examples we will choose a charged-Higgs mass of $m_{H^\pm} = 200$ GeV and the right-handed neutrino mass of $m_N = 200$ GeV. As the Z boson couples strongly to left-handed (right-handed) electron (positron) compared to right-handed electron, left polarized electron, and right polarized positron beam enhances the H^+H^- cross-section. We study the effect of beam polarization by comparing the results for unpolarized beams to those with $P_{e^\pm} = +30\%$ and $P_{e^\pm} = -50\%$. The plots of the total cross section as a function of the CM energy are presented in fig. 11.

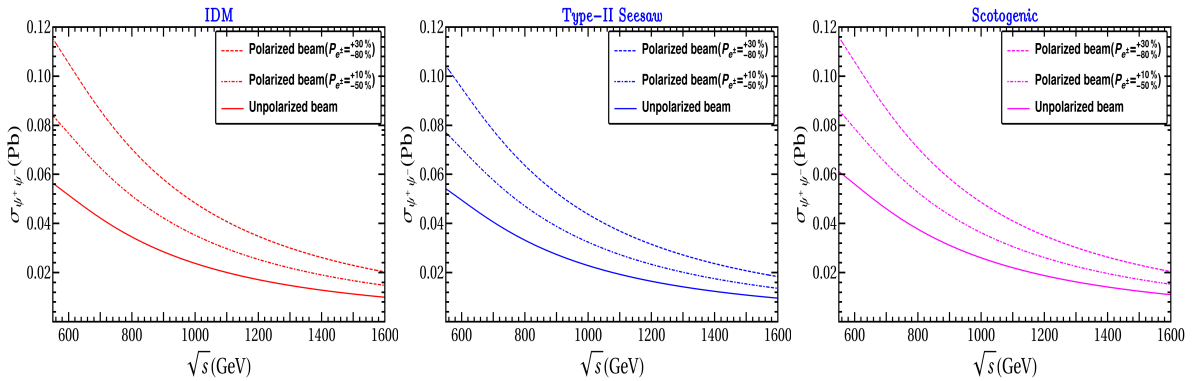


Figure 11: The total cross-section for charged scalar pair production as a function of the CM energy (\sqrt{s}) at an e^+e^- collider for unpolarized beams and two different choices of beam polarization. Left: IDM; middle: type-II seesaw; right: scotogenic (see eq. (4.4)).

4.3 Collider analysis of the inert doublet model

In this section we estimate the efficiency factor ϵ for H^+H^- production within the inert doublet model (IDM). This model is one of the simplest extension of the SM where the scalar sector is assumed to include an additional doublet H_2 , and an unbroken discrete \mathbb{Z}_2 symmetry under which H_2 is odd whereas all other fields are even. This discrete symmetry forbids Yukawa interactions between the inert doublet H_2 and SM fermions and ensures that the lightest physical component of H_2 can serve as a Dark Matter (DM) candidate. The Lagrangian consisting the scalar dark sector can be written as

$$\mathcal{L} = \mathcal{L}_{\text{SM}} + |D_\mu H_2|^2 - V(H_1, H_2), \quad (4.7)$$

where,

$$\begin{aligned} V(H_1, H_2) = & -\mu_H^2(H_1^\dagger H_1) + \lambda_H(H_1^\dagger H_1)^2 + \mu^2(H_2^\dagger H_2) + \lambda(H_2^\dagger H_2)^2 + \lambda_1(H_1^\dagger H_1)(H_2^\dagger H_2) \\ & + \lambda_2(H_1^\dagger H_2)(H_2^\dagger H_1) + \frac{\lambda_3}{2}[(H_1^\dagger H_2)^2 + \text{H.c.}]. \end{aligned} \quad (4.8)$$

We assume $\mu^2 > 0$ that ensures that the vacuum expectation value of the inert doublet vanishes and guarantees that \mathbb{Z}_2 remains unbroken. In contrast the SM scalar doublet H_1 does acquire a vacuum expectation value v . The physical modes consist of a singly-charged scalar H^\pm , a CP-odd neutral scalar A^0 , and CP-even neutrals h, H^0 , where h is the physical SM scalar field. The corresponding tree-level masses are given by

$$\begin{aligned} m_{H^0}^2 &= \mu^2 + \lambda_L v^2, \\ m_{H^\pm}^2 &= \mu^2 + \frac{1}{2}\lambda_1 v^2, \\ m_{A^0}^2 &= \mu^2 + \frac{1}{2}(\lambda_1 + \lambda_2 - 2\lambda_3)v^2, \end{aligned} \quad (4.9)$$

where $\lambda_L = \frac{1}{2}(\lambda_1 + \lambda_2 + \lambda_3)$.

The signal we will use to identify the production of an H^+H^- pair will be two opposite-sign e or μ leptons (OSL) plus missing energy (\cancel{E}). The decay chain can be written as

$$e^+e^- \rightarrow H^+H^-, \quad H^\pm \rightarrow H^0W^\pm, \quad W^- \rightarrow l^-\bar{\nu}_l, \quad W^+ \rightarrow l^+\nu_l; \quad (4.10)$$

where we focus on the leptonic decay modes of W . The dominant (non-interfering) SM background arises from W^+W^- , ZZ and W^+W^-Z production. The analysis of H^+H^- production in an e^+e^- collider for the IDM has been studied in detail in several publications, see, *e.g.*, [98–101].

We use the criteria for events reconstruction as in section 3.1 in order to reduce the SM background we impose the following cuts:

- \mathcal{C}_1 : events must contain two opposite sign leptons in the final state.

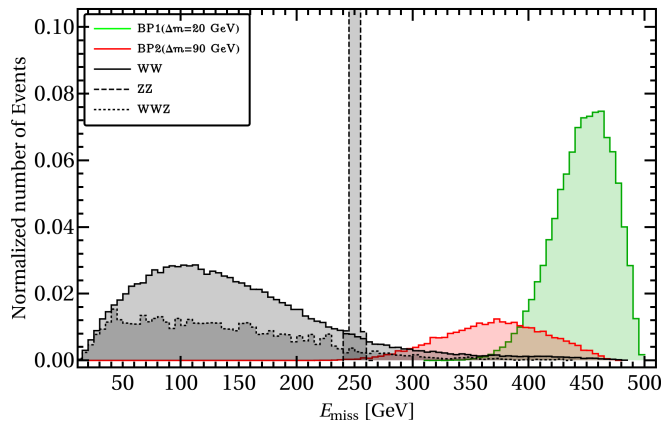


Figure 12: Normalized missing energy distribution of OSL + missing energy signal for IDM at the $e^+ e^-$ collider with $\sqrt{s} = 500$ GeV and unpolarized beams.

BPs	Δm	m_{H^\pm}	Cross-section (fb)	
			$P_{e^\pm} = 0$	$P_{e^\pm} = \begin{smallmatrix} +30\% \\ -80\% \end{smallmatrix}$
BP1	20	90	101.2	201.2
BP2	90	160	56.5	112.4

Table 4: Total cross-section of charged scalar pair-production ($H^+ H^-$) for different benchmark points for unpolarized and polarized ($P_{e^\pm} = \begin{smallmatrix} +30\% \\ -80\% \end{smallmatrix}$) beams.

- \mathcal{C}_2 : missing energy $\cancel{E} \leq 370$ (300) for BP1 (BP2).

It follows from fig. 12 that $\mathcal{C}_{1,2}$ strongly reduce the (non-interfering) SM backgrounds. We also chose charged scalar masses equal to $m_{H^\pm} = 90$ GeV and 160 GeV in view of the latest bounds [102]. Using the definition of ϵ in eq. (3.11), the efficiency factor for the two benchmark points is tabulated in table 5. These results justify the conservative choice $\epsilon = 0.005$ we used above for all the different NP scenarios.

4.4 1σ surfaces in the $a - b$ plane

We now apply the OOT to obtain the optimal statistical uncertainty regions for the NP couplings (a, b); the results are presented in table 6 and the corresponding 1σ regions are shown in fig. 13 with CM energy (\sqrt{s}) = 500 GeV, luminosity (\mathcal{L}_{int}) = 1000 fb $^{-1}$ and signal efficiency (ϵ) = 0.005. For the IDM and type II models the uncertainties in NP couplings are similar since the cross sections are almost equal. For the scotogenic model where $b \neq 0$, the t-channel diagram contributes and enhances the cross section, resulting in an increased sensitivity to b . In table 6, 1σ uncertainties of NP couplings for two different charged Higgs masses ($m_{H^\pm} = 90, 160$ GeV) are listed. For $m_{H^\pm} = 160$ GeV, due to smaller production

Cuts	Cross-section					Efficiency factor (ϵ)	
	Signal		SM background				
	BP1 (fb)	BP2 (fb)	$W^+ W^-$ (fb)	ZZ (fb)	$W^+ W^- Z$ (fb)	ϵ^{BP1}	ϵ^{BP2}
\mathcal{C}_1	2.02	1.13	211.4	11.2	0.8	0.02	0.02
\mathcal{C}_2	1.96	0.85	4.01	0.0	0.002	0.019	0.015

Table 5: Event cross-section and efficiency factor (ϵ) for two different benchmark points of IDM and corresponding SM background estimation background estimation for unpolarized beams with CM energy (\sqrt{s}) = 500 GeV.

cross-section, the uncertainties of NP couplings are increased by $\sim 30\%$ compared to the case of $m_{H^\pm} = 90$ GeV. We can also see that a judicious choice of polarization also enhances the cross section, leading to a reduced statistical uncertainty in the determination of the NP coefficients. For $P_{e^\pm} = {}^{+30\%}_{-80\%}$ the uncertainty in the parameter a (b) is reduced by $\sim 50\text{-}55\%$ ($\sim 25\text{-}40\%$). Finally, as a function of the luminosity \mathcal{L} and the efficiency ϵ , the uncertainties scale as $1/(\sqrt{\mathcal{L}_{int}\epsilon})$ with the expected result that a larger luminosity and/or efficiency also lead to reduction of the uncertainties.

4.5 Differentiation of models

We can now follow the same approach as in section 3.3 and use the OOT to estimate the extent to which different hypotheses can be distinguished. Specifically, given a “base” and alternate hypotheses, $\{a^0, b^0\}$ and $\{\bar{a}, \bar{b}\}$, respectively, we define the significance as in eq. (3.12) (where now $g_i^0 = g_i(a^0, b^0)$, $\bar{g}_i = g_i(\bar{a}, \bar{b})$) and again assume that these hypotheses can be distinguished at the $\geq \ell\sigma$ level if $\Delta\sigma \geq \ell$.

Taking $a^0 = b^0 = 0$ (similar to the SM) as a base hypothesis, we determine the statistical separation of the models listed above. For CM energy $\sqrt{s} = 500$ GeV, $\mathcal{L}_{int} = 1000$ fb $^{-1}$, $m_{H^\pm} = 160$ GeV, and $\epsilon = 0.005$, the separation significance are listed in table 7 and corresponding plots are shown in fig. 14. For unpolarized beams, we can see that for both inert doublet and type-II seesaw models are under discovery limit (that is, $\Delta\sigma < 5$), but the scotogenic model is above this limit due to the enhancement of the cross-section by the t-channel N_R contribution. Polarized beams ($P_{e^\pm} = {}^{+30\%}_{-80\%}$) enhances the production cross-section, which in turn provides a clear distinction (above 5σ) of the three different models from the base hypothesis. Also note that with larger luminosity, total number of events increases to provide higher significance.

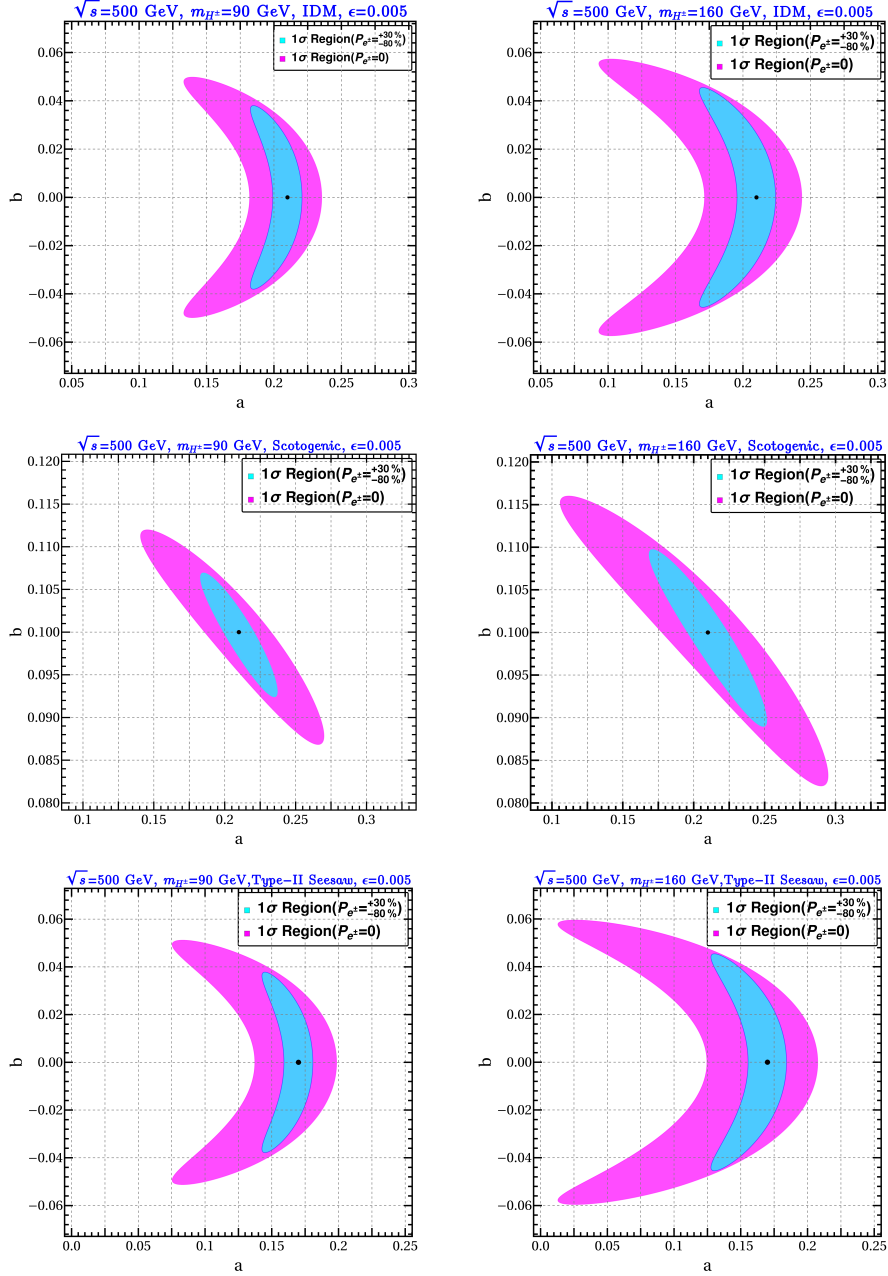


Figure 13: Optimal 1σ surfaces for different models with unpolarized and polarized beams $P_{e^\pm} = +30\%/-80\%$, $\epsilon = 0.005$, and $m_{H^\pm} = 90$ GeV (left column) or $m_{H^\pm} = 160$ GeV (right column).

4.6 Comparison between optimal and standard χ^2

The statistical uncertainties obtained using the OOT can be compared to those obtained using a basic collider analysis based on eq. (3.13), as was done in section 3.4. Here also

		Uncertainties			
		$P_{e^\pm} = 0$		$P_{e^\pm} = \begin{smallmatrix} +30\% \\ -80\% \end{smallmatrix}$	
Model	$m_{H^\pm}(\text{GeV})$	$\pm\Delta a$	$\pm\Delta b$	$\pm\Delta a$	$\pm\Delta b$
Inert doublet	90	+0.025	+0.050	+0.011	+0.038
		-0.077	-0.050	-0.027	-0.038
	160	+0.033	+0.058	+0.014	+0.046
		-0.117	-0.058	-0.042	-0.046
Scotogenic	90	+0.060	+0.012	+0.028	+0.007
		-0.070	-0.012	-0.028	-0.007
	160	+0.085	+0.016	+0.041	+0.010
		-0.105	-0.016	-0.042	-0.010
Type-II Seesaw	90	+0.028	+0.050	+0.017	+0.038
		-0.095	-0.050	-0.028	-0.038
	160	+0.037	+0.058	+0.015	+0.046
		-0.157	-0.058	-0.043	-0.046

Table 6: Optimal 1σ statistical uncertainty in the a, b couplings for both unpolarized and polarized $P_{e^\pm} = \begin{smallmatrix} +30\% \\ -80\% \end{smallmatrix}$ beams with $\epsilon = 0.005$.

Models	significance ($\Delta\sigma$)	
	$P_{e^\pm} = 0$	$P_{e^\pm} = \begin{smallmatrix} +30\% \\ -80\% \end{smallmatrix}$
Inert doublet	4σ	17σ
Type-II Seesaw	2.82σ	13σ
Scotogenic	17σ	40σ

Table 7: Statistical significance of three different models with respect to the $a^0 = b^0 = 0$ model.

we consider the differential cross-section for H^+H^- pair production after subsequent decays (with the same cuts as in section 4.3) to OSL + missing energy for the binned analysis. The resulting 1σ regions in the $a - b$ plane for three different models are shown in fig. 15 for both the binned and OOT analyses (the collider parameters as in section 4.3). The 1σ contours for binned analysis (OOT) are shown by green (pink) color contours. In this scenario, with purely NP productions, the cross-section is larger, statistical fluctuation in each bin is less,

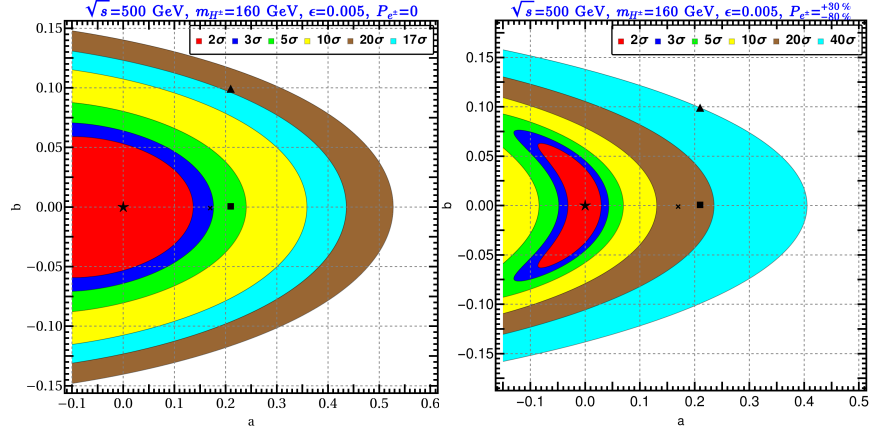


Figure 14: Statistical significance of alternate models with respect to the $a^0 = b^0 = 0$ model (*cf.* eq. (3.12)), $\Delta\sigma \leq \ell$, for various choices of ℓ . Cross, square and triangle correspond to the IDM, type-II seesaw and scotogenic models, respectively. Left: unpolarized beams, right: polarized beams $P_{e^\pm} = \begin{matrix} +30\% \\ -80\% \end{matrix}$.

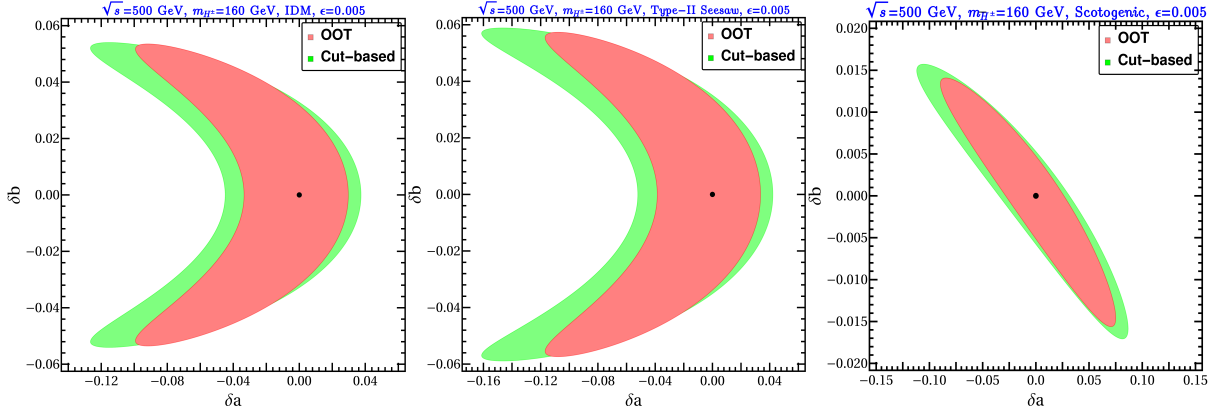


Figure 15: Comparison of 1σ statistical limit for OOT (pink) and collider (green) χ^2 in $a - b$ plane for charged scalar pair production at e^+e^- colliders for unpolarized beam. All the relevant parameters are written in the caption. Left: IDM; middle: type-II seesaw; right: scotogenic model (see eq. (4.4)).

making the NP uncertainties determined through binned analysis close to OOT.

5 Summary and Conclusions

The OOT determines the smallest statistical uncertainty with which a NP coupling can be extracted from experiment. In this work we studied two limits of this technique, one in SMEFT ($t\bar{t}$ production in an e^+e^- collider) where the SM dominates over the NP contribution, and one in UV complete NP models (H^+H^- production in an e^+e^- collider) where SM contribution is subdominant.

For the first application we used an effective Lagrangian parameterization of the NP effects, including for simplicity only those operators that do not interfere with the SM contributions in this process. We find that for realistic collider parameters the 1σ statistical uncertainty of the NP parameters lie in the 20% to 100% range (depending on the values of the coefficients, the beam polarizations and the efficiency of signal background estimation). The possibility of distinguishing different NP models (defined by their values of the NP coefficients) is equally modest, with a significance below 5σ in all cases studied.

In the second application the NP particles are assumed to be light enough to be directly produced. Here we find that the sensitivity is much higher so that the NP parameters could be measured to a precision of 1% to 10% (depending on the values of the coefficients, the beam polarizations and the efficiency). Moreover, different models can be easily distinguished, provided the beams are strongly polarized, which provides a useful comparison of how efficiently the NP couplings can be extracted at the proposed future e^+e^- colliders. The calculations for both applications require the estimation of an efficiency factor ϵ which we obtain by performing standard collider analyses of the corresponding reactions by studying a cut based signal background analysis.

The statistical uncertainties in the NP coefficients obtained using the OOT are $O(0.5)$ in the first case we considered (section 3), while significantly smaller, $O(0.05)$, for the second example (section 4). This is imply due to the different values of the NP contributions to the cross sections in each case: in the first the NP effects are small, this leads to a relatively small inverse-correlation matrix M in eq. (2.2), while in the second example NP effects dominate leading to a larger M and correspondingly smaller uncertainties.

We also compared the OOT results with those obtained a simple collider estimate of the parameter uncertainties based on the χ^2 statistic of eq. (3.13). We found that the optimal uncertainties are significantly smaller in the case where the NP effects are subdominant, but that in the case where the NP dominates the results are comparable. The collider analysis, however, can be improved by optimizing the data binning, and possibly by selecting a better suited statistic; such investigations, however, lie outside the scope of this paper.

Acknowledgments

SB would like to acknowledge the grant CRG/2019/004078 from DST-SERB, Govt. of India. SJ thanks Jayita Lahiri for useful discussions.

A OOT for large NP

In this appendix we provide a derivation of the correlation matrix that determines the optimal statistical uncertainties of the model parameters. We interpret the differential cross section $d\sigma/d\phi$ (where ϕ denote the relevant phase-space coordinates) as an unnormalized probability density function; its normalized counterpart is then

$$f_{\text{theo}} = \frac{1}{\Sigma_{\text{theo}}} \frac{d\sigma}{d\phi}; \quad \Sigma_{\text{theo}} = \left\langle \frac{d\sigma}{d\phi} \right\rangle, \quad (\text{A.1})$$

where, for any $X(\phi)$,

$$\langle X \rangle = \int d\phi X(\phi). \quad (\text{A.2})$$

Denoting by $\mathfrak{L}_{\text{int}}$ the integrated luminosity over a period, the average event number in that period is

$$\mathfrak{N} = \mathfrak{L}_{\text{int}} \Sigma_{\text{theo}}. \quad (\text{A.3})$$

Assuming the events occur at a constant rate and are independent of one another⁹, the probability of observing A events is given by a Poisson distribution

$$\frac{\mathfrak{N}^A}{A!} e^{-\mathfrak{N}}. \quad (\text{A.4})$$

Therefore the probability of observing A events in regions $\Delta\phi_a$ around phase-space points ϕ_a , $a = 1, \dots, A$ is

$$\begin{aligned} \mathfrak{P}(A; \boldsymbol{\xi}_A) \Delta\boldsymbol{\xi}_A &= \frac{\mathfrak{N}^A}{A!} e^{-\mathfrak{N}} \prod_{a=1}^A f_{\text{theo}}(\phi_a) \Delta\phi_a; \quad \boldsymbol{\xi}_A = (\phi_1, \dots, \phi_A), \quad \Delta\boldsymbol{\xi}_A = \prod_{a=1}^A \Delta\phi_a, \\ \Rightarrow \mathfrak{P}(A; \boldsymbol{\xi}_A) &= \frac{e^{-\mathfrak{N}}}{A!} \prod_{a=1}^A \mathfrak{f}_{\text{theo}}(\phi_a); \quad \mathfrak{f}_{\text{theo}} = \mathfrak{N}_{\text{theo}} f_{\text{theo}} = \mathfrak{L}_{\text{int}} \frac{d\sigma_{\text{theo}}}{d\phi}. \end{aligned} \quad (\text{A.5})$$

Now, for all cases of interest the cross-section can be written in form

$$\frac{d\sigma_{\text{theo}}}{d\phi} = \mathbf{g} \cdot \mathbf{f}(\phi), \quad (\text{A.6})$$

⁹Situations where this may not be true usually occur when the number of events is very large, so that effects such as Bose enhancement of Pauli blocking become important.

where $\mathbf{g} = (g_1, \dots, g_n)$ are a set of parameters to be determined through observations, and \mathbf{f} a set of convenient linearly-independent phase-space functions¹⁰ The coefficients g_i will be (not necessarily linear) functions of the Lagrangian parameters and, for processes that receive SM contributions, some or all of them will depend on the SM parameters. We make no additional assumptions on the magnitude of the g_i .

The goal is to obtain a set observables that allow the determination of the \mathbf{g} with the smallest statistical uncertainty possible. To do this we first choose a generic set of observables $\mathcal{O}_i(\phi)$, ($i = 1, \dots, n$) and let

$$\mathcal{O}_i(A; \boldsymbol{\xi}_A) = \sum_{a=1}^A \mathcal{O}_i(\phi_a). \quad (\text{A.7})$$

Then

$$\left(\mathfrak{P} \mathcal{O}_i \right) = \sum_{A=1}^{\infty} \frac{e^{-\mathfrak{N}}}{A!} \mathfrak{N}^{A-1} A \langle \mathfrak{f}_{\text{theo}} \mathcal{O}_i \rangle = \langle \mathfrak{f}_{\text{theo}} \mathcal{O}_i \rangle = \mathfrak{L}_{\text{int}} \langle \mathcal{O}_i f_j \rangle g_j, \quad (\text{A.8})$$

where, given a function $\mathcal{U}(\boldsymbol{\xi}_A)$,

$$\left(\mathcal{U} \right) = \sum_{A=1}^{\infty} \frac{e^{-\mathfrak{N}}}{A!} \int d\boldsymbol{\xi}_A \mathcal{U}(\boldsymbol{\xi}_A). \quad (\text{A.9})$$

Let then

$$\Gamma_i = C_{ij}^{-1} \mathcal{O}_j, \quad C_{ij} = \mathfrak{L}_{\text{int}} \langle \mathcal{O}_i f_j \rangle \Rightarrow g_i = \left(\mathfrak{P} \Gamma_i \right), \quad (\text{A.10})$$

so the Γ_i can be used to determine the g_i . The correlation matrix of these observables is given by

$$V_{ij} = \left(\mathfrak{P} \Gamma_i \Gamma_j \right) - g_i g_j, \quad (\text{A.11})$$

which we extremize as a function of the \mathcal{O}_i :

$$\frac{\delta V_{ij}}{\delta \mathcal{O}_k} = 0. \quad (\text{A.12})$$

A straightforward calculation shows that the solution is

$$\mathcal{O}_k = \frac{f_k}{\mathfrak{f}_{\text{theo}}}, \quad (\text{A.13})$$

for which the condition $\langle f_k \rangle = C_{kl} g_l$ is satisfied and

$$V = \frac{1}{\mathfrak{L}_{\text{int}}} C^{-1}; \quad C_{ij} = \mathfrak{L}_{\text{int}} \left\langle \frac{f_i f_j}{\mathfrak{f}_{\text{theo}}} \right\rangle = \left\langle \frac{f_i f_j}{(d\sigma/d\phi)} \right\rangle. \quad (\text{A.14})$$

If the cross section receives a contribution from both the SM and the new physics, and when the relevant SM parameters are well measured we write

$$\frac{d\sigma}{d\phi} = \frac{d\sigma_{\text{MS}}}{d\phi} + \mathbf{g} \cdot \mathbf{f}(\phi) \quad (\text{A.15})$$

where the second term contains pure NP contributions, and, in general, SM-NP interference terms as well. In this case a similar derivation to the one above gives again eq. (A.14).

¹⁰The choice of f_i is not unique, but all observable results are unambiguous [15].

References

- [1] ATLAS collaboration, *Observation of a new particle in the search for the Standard Model Higgs boson with the ATLAS detector at the LHC*, *Phys. Lett. B* **716** (2012) 1 [[1207.7214](#)].
- [2] CMS collaboration, *Observation of a New Boson at a Mass of 125 GeV with the CMS Experiment at the LHC*, *Phys. Lett. B* **716** (2012) 30 [[1207.7235](#)].
- [3] *The International Linear Collider Technical Design Report - Volume 1: Executive Summary*, [1306.6327](#).
- [4] *The International Linear Collider Technical Design Report - Volume 2: Physics*, [1306.6352](#).
- [5] ILC collaboration, *The International Linear Collider. A Global Project*, [1901.09829](#).
- [6] CLICDP, CLIC collaboration, *The Compact Linear Collider (CLIC) - 2018 Summary Report*, [1812.06018](#).
- [7] CLIC, CLICDP collaboration, *The Compact Linear e^+e^- Collider (CLIC): Physics Potential*, [1812.07986](#).
- [8] CLIC ACCELERATOR collaboration, *The Compact Linear Collider (CLIC) - Project Implementation Plan*, [1903.08655](#).
- [9] M. Ahmad et al., *CEPC-SPPC Preliminary Conceptual Design Report. 1. Physics and Detector*, .
- [10] *CEPC-SPPC Preliminary Conceptual Design Report. 2. Accelerator*, .
- [11] TLEP DESIGN STUDY WORKING GROUP collaboration, *First Look at the Physics Case of TLEP*, *JHEP* **01** (2014) 164 [[1308.6176](#)].
- [12] FCC collaboration, *FCC-ee: The Lepton Collider: Future Circular Collider Conceptual Design Report Volume 2*, *Eur. Phys. J. ST* **228** (2019) 261.
- [13] D. Atwood and A. Soni, *Analysis for magnetic moment and electric dipole moment form-factors of the top quark via $e^+e^- \rightarrow t\bar{t}$* , *Phys. Rev. D* **45** (1992) 2405.
- [14] M. Davier, L. Duflot, F. Le Diberder and A. Rouge, *The Optimal method for the measurement of tau polarization*, *Phys. Lett. B* **306** (1993) 411.
- [15] M. Diehl and O. Nachtmann, *Optimal observables for the measurement of three gauge boson couplings in $e^+e^- \rightarrow W^+W^-$* , *Z. Phys. C* **62** (1994) 397.
- [16] J. F. Gunion, B. Grzadkowski and X.-G. He, *Determining the $t\bar{t}$ and ZZ couplings of a neutral Higgs boson of arbitrary CP nature at the NLC*, *Phys. Rev. Lett.* **77** (1996) 5172 [[hep-ph/9605326](#)].
- [17] K. Hagiwara, S. Ishihara, J. Kamoshita and B. A. Kniehl, *Prospects of measuring general Higgs couplings at e^+e^- linear colliders*, *Eur. Phys. J. C* **14** (2000) 457 [[hep-ph/0002043](#)].
- [18] S. Dutta, K. Hagiwara and Y. Matsumoto, *Measuring the Higgs-Vector boson Couplings at Linear e^+e^- Collider*, *Phys. Rev. D* **78** (2008) 115016 [[0808.0477](#)].
- [19] Z. Hioki, T. Konishi and K. Ohkuma, *Studying possible CP-violating Higgs couplings through top-quark pair productions at muon colliders*, *JHEP* **07** (2007) 082 [[0706.4346](#)].

- [20] B. Grzadkowski and Z. Hioki, *CP violating lepton energy correlation in $e^-e^+ \rightarrow t\bar{t}$* , *Phys. Lett. B* **391** (1997) 172 [[hep-ph/9608306](#)].
- [21] B. Grzadkowski, Z. Hioki and M. Szafranski, *Four Fermi effective operators in top quark production and decay*, *Phys. Rev. D* **58** (1998) 035002 [[hep-ph/9712357](#)].
- [22] B. Grzadkowski and Z. Hioki, *Probing top quark couplings at polarized NLC*, *Phys. Rev. D* **61** (2000) 014013 [[hep-ph/9805318](#)].
- [23] B. Grzadkowski and J. Pliszka, *Testing top quark Yukawa interactions in $e^+e^- \rightarrow t\bar{t}Z$* , *Phys. Rev. D* **60** (1999) 115018 [[hep-ph/9907206](#)].
- [24] B. Grzadkowski and Z. Hioki, *Optimal observable analysis of the angular and energy distributions for top quark decay products at polarized linear colliders*, *Nucl. Phys. B* **585** (2000) 3 [[hep-ph/0004223](#)].
- [25] B. Grzadkowski, Z. Hioki, K. Ohkuma and J. Wudka, *Optimal-observable analysis of possible new physics using the b quark in $\gamma\gamma \rightarrow t\bar{t} \rightarrow bX$* , *Phys. Lett. B* **593** (2004) 189 [[hep-ph/0403174](#)].
- [26] B. Grzadkowski, Z. Hioki, K. Ohkuma and J. Wudka, *Optimal beam polarizations for new-physics search through $\gamma\gamma \rightarrow t\bar{t} \rightarrow lX/bX$* , *JHEP* **11** (2005) 029 [[hep-ph/0508183](#)].
- [27] Q.-H. Cao and J. Wudka, *Search for new physics via single top production at TeV energy e gamma colliders*, *Phys. Rev. D* **74** (2006) 094015 [[hep-ph/0608331](#)].
- [28] J. F. Gunion and J. Pliszka, *Determining the relative size of the CP even and CP odd Higgs boson couplings to a fermion at the LHC*, *Phys. Lett. B* **444** (1998) 136 [[hep-ph/9809306](#)].
- [29] Z. Hioki and K. Ohkuma, *Optimal-observable Analysis of Possible Non-standard Top-quark Couplings in $pp \rightarrow t\bar{t}X \rightarrow l^+X'$* , *Phys. Lett. B* **716** (2012) 310 [[1206.2413](#)].
- [30] Z. Hioki and K. Ohkuma, *Final charged-lepton angular distribution and possible anomalous top-quark couplings in $pp \rightarrow t\bar{t}X \rightarrow \ell^+X'$* , *Phys. Lett. B* **736** (2014) 1 [[1406.2475](#)].
- [31] S. Bhattacharya, S. Nandi and S. K. Patra, *Optimal-observable analysis of possible new physics in $B \rightarrow D^{(*)}\tau\nu_\tau$* , *Phys. Rev. D* **93** (2016) 034011 [[1509.07259](#)].
- [32] Z. Calcuttawala, A. Kundu, S. Nandi and S. K. Patra, *Optimal observable analysis for the decay $b \rightarrow s$ plus missing energy*, *Eur. Phys. J. C* **77** (2017) 650 [[1702.06679](#)].
- [33] Z. Calcuttawala, A. Kundu, S. Nandi and S. Kumar Patra, *New physics with the lepton flavor violating decay $\tau \rightarrow 3\mu$* , *Phys. Rev. D* **97** (2018) 095009 [[1802.09218](#)].
- [34] S. Bhattacharya, S. Jahedi and J. Wudka, *Probing heavy charged fermions at e^+e^- collider using the optimal observable technique*, *JHEP* **05** (2022) 009 [[2106.02846](#)].
- [35] S. Jahedi and J. Lahiri, *Probing anomalous $ZZ\gamma$ and $Z\gamma\gamma$ Couplings at the e^+e^- Colliders using Optimal Observable Technique*, [2212.05121](#).
- [36] S. Jahedi, *Optimal estimation of Dimension-8 Neutral Triple Gauge Couplings at e^+e^- Colliders*, [2305.11266](#).
- [37] L. Holmstrom, S. R. Sain and H. E. Miettinen, *A New multivariate technique for top quark search*, *Comput. Phys. Commun.* **88** (1995) 195.
- [38] TMVA collaboration, *TMVA - Toolkit for Multivariate Data Analysis*, [physics/0703039](#).

- [39] H. Voss, A. Hocker, J. Stelzer and F. Tegenfeldt, *TMVA, the Toolkit for Multivariate Data Analysis with ROOT*, *PoS ACAT* (2007) 040.
- [40] P. C. Bhat, *Multivariate Analysis Methods in Particle Physics*, *Ann. Rev. Nucl. Part. Sci.* **61** (2011) 281.
- [41] D0 collaboration, *A precision measurement of the mass of the top quark*, *Nature* **429** (2004) 638 [[hep-ex/0406031](#)].
- [42] D0 collaboration, *Helicity of the W boson in lepton + jets $t\bar{t}$ events*, *Phys. Lett. B* **617** (2005) 1 [[hep-ex/0404040](#)].
- [43] F. Fiedler, A. Grohsjean, P. Haefner and P. Schieferdecker, *The Matrix Element Method and its Application in Measurements of the Top Quark Mass*, *Nucl. Instrum. Meth. A* **624** (2010) 203 [[1003.1316](#)].
- [44] P. Artoisenet, V. Lemaitre, F. Maltoni and O. Mattelaer, *Automation of the matrix element reweighting method*, *JHEP* **12** (2010) 068 [[1007.3300](#)].
- [45] J. F. Gunion, H. E. Haber, G. L. Kane and S. Dawson, *The Higgs Hunter's Guide*, vol. 80. 2000.
- [46] G. C. Branco, P. M. Ferreira, L. Lavoura, M. N. Rebelo, M. Sher and J. P. Silva, *Theory and phenomenology of two-Higgs-doublet models*, *Phys. Rept.* **516** (2012) 1 [[1106.0034](#)].
- [47] S. Weinberg, *Baryon and Lepton Nonconserving Processes*, *Phys. Rev. Lett.* **43** (1979) 1566.
- [48] W. Buchmuller and D. Wyler, *Effective Lagrangian Analysis of New Interactions and Flavor Conservation*, *Nucl. Phys. B* **268** (1986) 621.
- [49] B. Grzadkowski, M. Iskrzynski, M. Misiak and J. Rosiek, *Dimension-Six Terms in the Standard Model Lagrangian*, *JHEP* **10** (2010) 085 [[1008.4884](#)].
- [50] L. Lehman, *Extending the Standard Model Effective Field Theory with the Complete Set of Dimension-7 Operators*, *Phys. Rev. D* **90** (2014) 125023 [[1410.4193](#)].
- [51] S. Bhattacharya and J. Wudka, *Dimension-seven operators in the standard model with right handed neutrinos*, *Phys. Rev. D* **94** (2016) 055022 [[1505.05264](#)].
- [52] H.-L. Li, Z. Ren, J. Shu, M.-L. Xiao, J.-H. Yu and Y.-H. Zheng, *Complete set of dimension-eight operators in the standard model effective field theory*, *Phys. Rev. D* **104** (2021) 015026 [[2005.00008](#)].
- [53] C. W. Murphy, *Dimension-8 operators in the Standard Model Effective Field Theory*, *JHEP* **10** (2020) 174 [[2005.00059](#)].
- [54] C. W. Murphy, *Low-Energy Effective Field Theory below the Electroweak Scale: Dimension-8 Operators*, *JHEP* **04** (2021) 101 [[2012.13291](#)].
- [55] H.-L. Li, Z. Ren, M.-L. Xiao, J.-H. Yu and Y.-H. Zheng, *Complete set of dimension-nine operators in the standard model effective field theory*, *Phys. Rev. D* **104** (2021) 015025 [[2007.07899](#)].
- [56] Y. Liao and X.-D. Ma, *An explicit construction of the dimension-9 operator basis in the standard model effective field theory*, *JHEP* **11** (2020) 152 [[2007.08125](#)].

- [57] H.-L. Li, Z. Ren, M.-L. Xiao, J.-H. Yu and Y.-H. Zheng, *Low energy effective field theory operator basis at $d \leq 9$* , *JHEP* **06** (2021) 138 [[2012.09188](#)].
- [58] J. A. Aguilar-Saavedra, *Effective four-fermion operators in top physics: A Roadmap*, *Nucl. Phys. B* **843** (2011) 638 [[1008.3562](#)].
- [59] G. Durieux, F. Maltoni and C. Zhang, *Global approach to top-quark flavor-changing interactions*, *Phys. Rev. D* **91** (2015) 074017 [[1412.7166](#)].
- [60] A. Buckley, C. Englert, J. Ferrando, D. J. Miller, L. Moore, M. Russell et al., *Global fit of top quark effective theory to data*, *Phys. Rev. D* **92** (2015) 091501 [[1506.08845](#)].
- [61] A. Buckley, C. Englert, J. Ferrando, D. J. Miller, L. Moore, M. Russell et al., *Constraining top quark effective theory in the LHC Run II era*, *JHEP* **04** (2016) 015 [[1512.03360](#)].
- [62] C. Degrande, F. Maltoni, K. Mimasu, E. Vryonidou and C. Zhang, *Single-top associated production with a Z or H boson at the LHC: the SMEFT interpretation*, *JHEP* **10** (2018) 005 [[1804.07773](#)].
- [63] M. Chala, J. Santiago and M. Spannowsky, *Constraining four-fermion operators using rare top decays*, *JHEP* **04** (2019) 014 [[1809.09624](#)].
- [64] J. D’Hondt, A. Mariotti, K. Mimasu, S. Moortgat and C. Zhang, *Learning to pinpoint effective operators at the LHC: a study of the $t\bar{t}b\bar{b}$ signature*, *JHEP* **11** (2018) 131 [[1807.02130](#)].
- [65] D. Barducci et al., *Interpreting top-quark LHC measurements in the standard-model effective field theory*, [1802.07237](#).
- [66] N. P. Hartland, F. Maltoni, E. R. Nocera, J. Rojo, E. Slade, E. Vryonidou et al., *A Monte Carlo global analysis of the Standard Model Effective Field Theory: the top quark sector*, *JHEP* **04** (2019) 100 [[1901.05965](#)].
- [67] T. Neumann and Z. E. Sullivan, *Off-Shell Single-Top-Quark Production in the Standard Model Effective Field Theory*, *JHEP* **06** (2019) 022 [[1903.11023](#)].
- [68] F. Maltoni, L. Mantani and K. Mimasu, *Top-quark electroweak interactions at high energy*, *JHEP* **10** (2019) 004 [[1904.05637](#)].
- [69] I. Brivio, S. Bruggisser, F. Maltoni, R. Moutafis, T. Plehn, E. Vryonidou et al., *O new physics, where art thou? A global search in the top sector*, *JHEP* **02** (2020) 131 [[1910.03606](#)].
- [70] G. L. Kane, G. A. Ladinsky and C. P. Yuan, *Using the Top Quark for Testing Standard Model Polarization and CP Predictions*, *Phys. Rev. D* **45** (1992) 124.
- [71] L. Brzezinski, B. Grzadkowski and Z. Hioki, *Effects of nonstandard interactions for the energy spectrum of secondary leptons in $e^+e^- \rightarrow t\text{ anti-}t$* , *Int. J. Mod. Phys. A* **14** (1999) 1261 [[hep-ph/9710358](#)].
- [72] E. Boos, M. Dubinin, M. Sachwitz and H. J. Schreiber, *Probe of the Wtb coupling in $t\text{ anti-}t$ pair production at linear colliders*, *Eur. Phys. J. C* **16** (2000) 269 [[hep-ph/0001048](#)].
- [73] R. Röntsch and M. Schulze, *Probing top- Z dipole moments at the LHC and ILC*, *JHEP* **08** (2015) 044 [[1501.05939](#)].
- [74] P. Janot, *Top-quark electroweak couplings at the FCC-ee*, *JHEP* **04** (2015) 182 [[1503.01325](#)].

- [75] C. Englert and M. Russell, *Top quark electroweak couplings at future lepton colliders*, *Eur. Phys. J. C* **77** (2017) 535 [[1704.01782](#)].
- [76] G. Durieux, M. Perelló, M. Vos and C. Zhang, *Global and optimal probes for the top-quark effective field theory at future lepton colliders*, *JHEP* **10** (2018) 168 [[1807.02121](#)].
- [77] G. Durieux, J. Gu, E. Vryonidou and C. Zhang, *Probing top-quark couplings indirectly at Higgs factories*, *Chin. Phys. C* **42** (2018) 123107 [[1809.03520](#)].
- [78] R. Jafari, P. Eslami, M. Mohammadi Najafabadi and H. Khanpour, *Constraining the top quark effective field theory using the top quark pair production in association with a jet at future lepton colliders*, *Phys. Lett. B* **806** (2020) 135469 [[1909.00592](#)].
- [79] S. Bismann, C. Grunwald, G. Hiller and K. Kröninger, *Top and Beauty synergies in SMEFT-fits at present and future colliders*, *JHEP* **06** (2021) 010 [[2012.10456](#)].
- [80] V. D. Barger, J. L. Hewett and R. J. N. Phillips, *New Constraints on the Charged Higgs Sector in Two Higgs Doublet Models*, *Phys. Rev. D* **41** (1990) 3421.
- [81] Y. Grossman, *Phenomenology of models with more than two Higgs doublets*, *Nucl. Phys. B* **426** (1994) 355 [[hep-ph/9401311](#)].
- [82] A. G. Akeroyd and W. J. Stirling, *Light charged Higgs scalars at high-energy e^+e^- colliders*, *Nucl. Phys. B* **447** (1995) 3.
- [83] A. G. Akeroyd, *Nonminimal neutral Higgs bosons at LEP-2*, *Phys. Lett. B* **377** (1996) 95 [[hep-ph/9603445](#)].
- [84] A. G. Akeroyd, *Fermiophobic and other nonminimal neutral Higgs bosons at the LHC*, *J. Phys. G* **24** (1998) 1983 [[hep-ph/9803324](#)].
- [85] M. Aoki, S. Kanemura, K. Tsumura and K. Yagyu, *Models of Yukawa interaction in the two Higgs doublet model, and their collider phenomenology*, *Phys. Rev. D* **80** (2009) 015017 [[0902.4665](#)].
- [86] L. Wang, J. M. Yang and Y. Zhang, *Two-Higgs-doublet models in light of current experiments: a brief review*, *Commun. Theor. Phys.* **74** (2022) 097202 [[2203.07244](#)].
- [87] PARTICLE DATA GROUP collaboration, *Review of Particle Physics*, *PTEP* **2022** (2022) 083C01.
- [88] CMS collaboration, *Probing effective field theory operators in the associated production of top quarks with a Z boson in multilepton final states at $\sqrt{s} = 13$ TeV*, *JHEP* **12** (2021) 083 [[2107.13896](#)].
- [89] R. Vega and J. Wudka, *A Covariant method for calculating helicity amplitudes*, *Phys. Rev. D* **53** (1996) 5286 [[hep-ph/9511318](#)].
- [90] A. Belyaev, N. D. Christensen and A. Pukhov, *CalcHEP 3.4 for collider physics within and beyond the Standard Model*, *Comput. Phys. Commun.* **184** (2013) 1729 [[1207.6082](#)].
- [91] J. Alwall, R. Frederix, S. Frixione, V. Hirschi, F. Maltoni, O. Mattelaer et al., *The automated computation of tree-level and next-to-leading order differential cross sections, and their matching to parton shower simulations*, *JHEP* **07** (2014) 079 [[1405.0301](#)].
- [92] G. Cowan, *Statistical data analysis*. 1998.

- [93] G. Bhattacharyya and D. Das, *Scalar sector of two-Higgs-doublet models: A minireview*, *Pramana* **87** (2016) 40 [[1507.06424](#)].
- [94] M. Krawczyk, N. Darvishi and D. Sokolowska, *The Inert Doublet Model and its extensions*, *Acta Phys. Polon. B* **47** (2016) 183 [[1512.06437](#)].
- [95] N. G. Deshpande and E. Ma, *Pattern of Symmetry Breaking with Two Higgs Doublets*, *Phys. Rev. D* **18** (1978) 2574.
- [96] J. Schechter and J. W. F. Valle, *Neutrino Decay and Spontaneous Violation of Lepton Number*, *Phys. Rev. D* **25** (1982) 774.
- [97] E. Ma, *Verifiable radiative seesaw mechanism of neutrino mass and dark matter*, *Phys. Rev. D* **73** (2006) 077301 [[hep-ph/0601225](#)].
- [98] M. Aoki, S. Kanemura and H. Yokoya, *Reconstruction of Inert Doublet Scalars at the International Linear Collider*, *Phys. Lett. B* **725** (2013) 302 [[1303.6191](#)].
- [99] M. Hashemi, M. Krawczyk, S. Najjari and A. F. Żarnecki, *Production of Inert Scalars at the high energy e^+e^- colliders*, *JHEP* **02** (2016) 187 [[1512.01175](#)].
- [100] J. Kalinowski, W. Kotlarski, T. Robens, D. Sokolowska and A. F. Żarnecki, *Benchmarking the Inert Doublet Model for e^+e^- colliders*, *JHEP* **12** (2018) 081 [[1809.07712](#)].
- [101] J. Kalinowski, W. Kotlarski, T. Robens, D. Sokolowska and A. F. Żarnecki, *Exploring Inert Scalars at CLIC*, *JHEP* **07** (2019) 053 [[1811.06952](#)].
- [102] A. Pierce and J. Thaler, *Natural Dark Matter from an Unnatural Higgs Boson and New Colored Particles at the TeV Scale*, *JHEP* **08** (2007) 026 [[hep-ph/0703056](#)].